as determined by enzyme-linked immunosorbent assay (ELISA) (Fig. 3B). We additionally examined the activation of endogenous IRF-3 by performing gel-shift assays. Expression of RIG-I(1–250) promoted the hallmarks of IRF-3 activation, namely, its dimerization and phosphorylation (Fig. 3C), both of which were impaired by Mfn2 in a dose-dependent manner (Fig. 3C).

Overexpression of Mfn2 additionally abrogated the effect of MDA-5 in a dose-dependent manner (Fig. 3D). MDA-5 is the intracellular receptor for poly(I:C), a synthetic analog of viral double-stranded RNA (*26*, *27*). Consistent with previous findings, the delivery of poly(I:C) into HEK 293 cells by transient transfection stimulated the IFN-β response, which was suppressed by Mfn2 (Fig. 3E). In contrast, Mfn2 did not impair the IFN-β response to extracellular poly(I:C) (Fig. 3E). Taken together, these results indicate that Mfn2 acted as a negative regulator of RIG-I–, MDA-5–, and dsRNA-dependent antiviral signaling through MAVS and suggested that the association of MAVS and Mfn2 might underlie this inhibition.

Loss of endogenous Mfn2 results in enhanced RIG-I– and MDA-5–induced antiviral responses

The previous experiments showed that Mfn2 suppressed MAVS-dependent signaling. We therefore attempted to determine, through an RNA interference

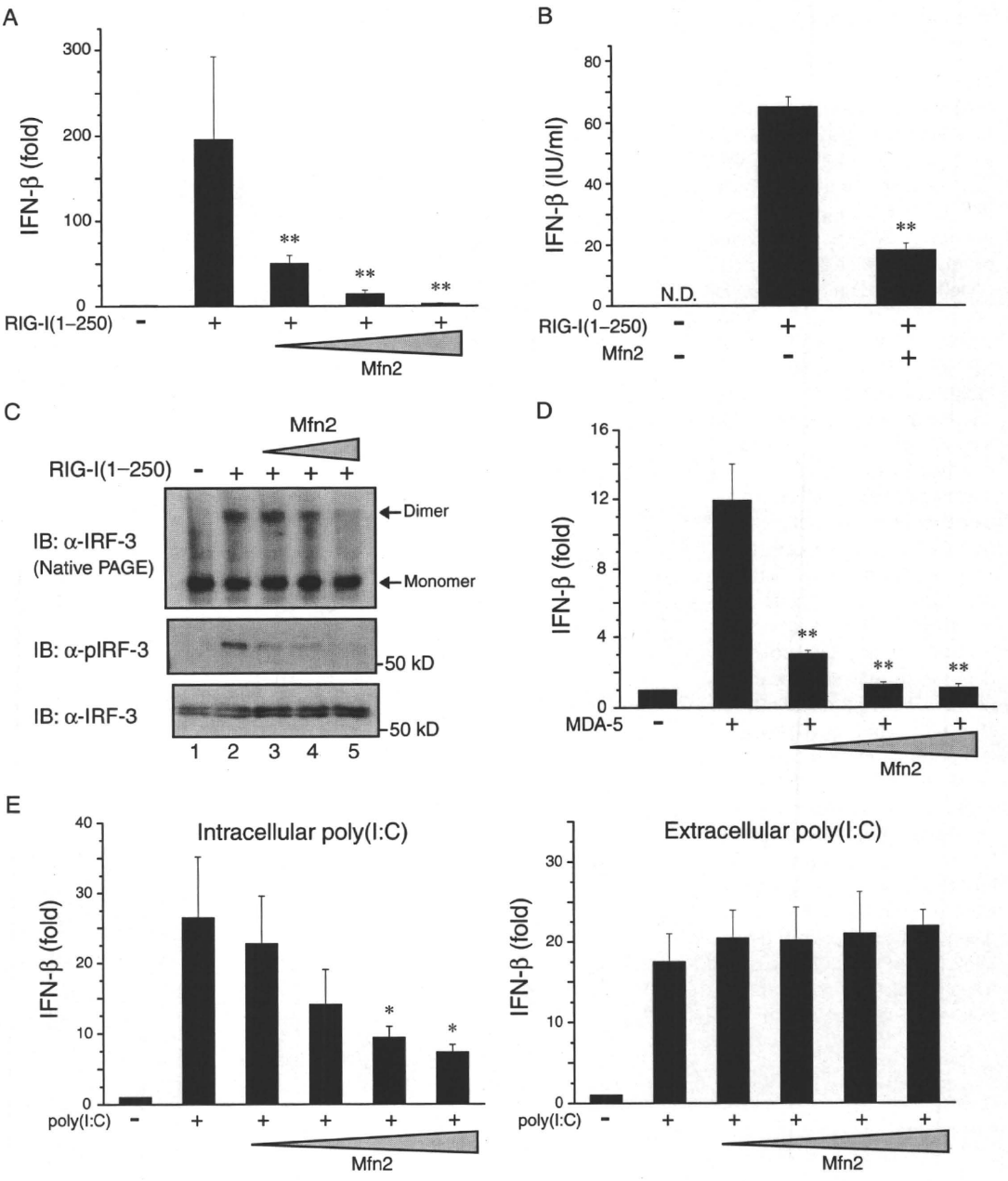

Fig. 3. Mfn2 suppresses IFN-β signaling mediated by RIG-I and MDA-5. (**A**) HEK 293 cells were cotransfected with 50 ng of plasmid encoding RIG-I(1–250) with increasing amounts (20, 50, and 100 ng) of a plasmid encoding Mfn2 together with the luciferase reporter plasmid p125luc. Transfected cells were analyzed 24 hours later for IFN-β–dependent luciferase activity. (**B**) HEK 293 cells were cotransfected with 200 ng of plasmid encoding RIG-I(1–250) and 200 ng of a plasmid encoding either pcDNA3.1 (negative) or Mfn2. Culture supernatants were harvested 24 hours after transfection and analyzed by ELISA to measure the production of IFN-β. (**C**) HEK 293 cells were cotransfected with 300 ng of a plasmid encoding RIG-I(1–250) and increasing amounts (100, 300, and 500 ng) of the plasmid encoding Mfn2. Cell lysates were resolved by electrophoresis under native (top panel) or denaturing conditions (middle and bottom panels) and then analyzed by Western blotting with the indicated antibodies. (**D**) Experiments were performed similarly to those in (A), except that the plasmid encoding MDA-5 was used in the transfections instead of the plasmid encoding RIG-I(1–250). (**E**) HEK 293 cells were transfected with various amounts (20, 50, 100, and 200 ng) of the plasmid encoding Mfn2 and were either cotransfected with poly(I:C) (left panel) or treated extracellularly with poly(I:C) (right panel). The resulting IFN-β reporter activity was determined as described earlier. All data shown represent mean values ± SD ($n = 3$ experiments). $^*P < 0.05$; $^{**}P < 0.01$.

approach, whether endogenous Mfn2 was responsible for modulating the MAVS-dependent transcriptional activation of the gene encoding IFN-β. Consistent with our previous findings, HEK 293 cells that had been treated with Mfn2-specific small interfering RNA (siRNA), which efficiently knocked down the amount of endogenous Mfn2 protein by greater than 90% (Fig. 4, A and B), exhibited enhanced induction of the IFN-β reporter construct in response to RIG-I(1–250) relative to that of control siRNA–transfected cells (Fig. 4B). Moreover, reintroduction of Myc-tagged Mfn2 into HEK 293 cells that had been treated with Mfn2-specific siRNA restored the suppressive effect on RIG-I(1–250)–dependent induction of the IFN-β reporter (Fig. 4C). HEK 293 cells also exhibited a differential response to an increased abundance of MAVS when treated with the Mfn2-specific siRNA, with increased activation of the IFN-β reporter and production of endogenous IFN-β relative to that of cells treated with the control siRNA (fig. S2, A and B). Knockdown of endogenous Mfn2 by siRNA similarly enhanced the activation of the IFN-β reporter and the production of IFN-β

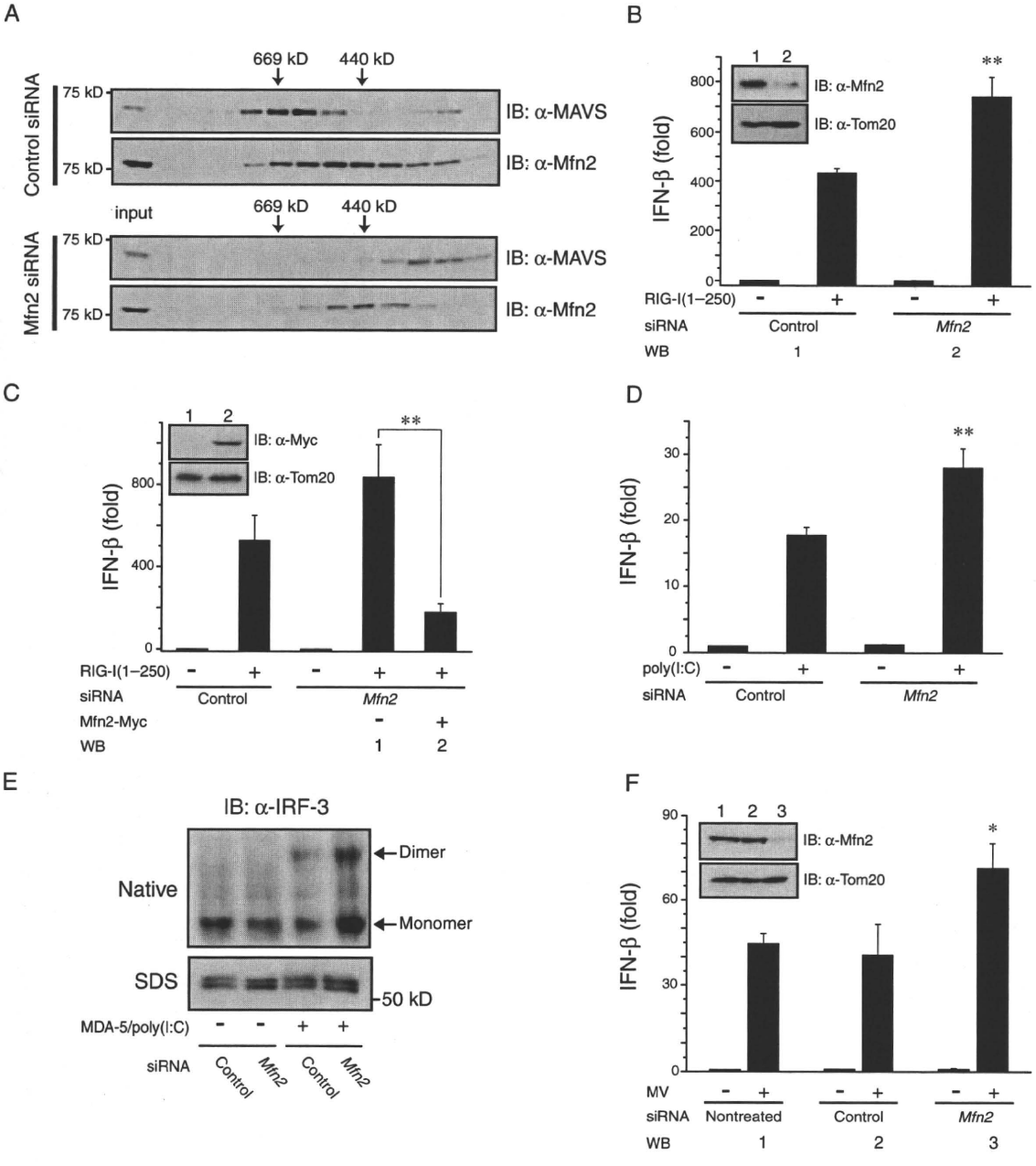

Fig. 4. Treatment with Mfn2-specific siRNA results in an enhanced antiviral response. (A) Gel filtration (Superose 6 HR-10/30) elution profiles of endogenous Mfn2 (as well as MAVS) extracted from the mitochondrial fraction of HEK 293 cells that had been treated with either control siRNA or siRNA specific for Mfn2. The positions corresponding to the elution of 669- and 440-kD molecular mass markers are indicated, and fractions were analyzed by Western blotting with antibodies against Mfn2 and MAVS. (B) HEK 293 cells were transfected with either control siRNA or siRNA specific for Mfn2 to evaluate the effect of knockdown of Mfn2 on the antiviral response. Twenty-four hours later, siRNA-treated cells were retransfected with the IFN-β reporter plasmid together with a plasmid encoding RIG-I(1–250). The efficiency of knockdown of Mfn2 (inset, lane 2) was confirmed by analysis of Western blots (WB) with a monoclonal antibody against Mfn2, and Tom20 was used as a loading control. (C) Experiments were performed similarly to those described in (B), except that IFN-β reporter-dependent luciferase activity was additionally measured after reintroduction of Myc-tagged Mfn2. Expression of the plasmid encoding Myc-tagged Mfn2 was confirmed by Western blotting analysis with an antibody (9E10) against Myc (inset, lane 2). (D) Experiments were performed similarly to those in (B), except that cells were transfected with poly(I:C) instead of the plasmid encoding RIG-I(1–250). (E) Knockdown of Mfn2 enhanced MDA-5–induced activation of IRF-3. (F) Activation of the IFN-β reporter in siRNA-treated HEK 293 cells infected with measles virus (MV) at an MOI of 2. All data shown represent mean values ± SD (n = 3 experiments). *P < 0.05; **P < 0.01.

protein in response to transfection with poly(I:C) (Fig. 4D and fig. S3), as well as increasing the amount of MDA-5–induced dimerized IRF-3 (Fig. 4E). Consistent with these findings, activation of the IFN-β reporter in response to infection with measles virus (MV), an RNA virus of the *Paramyxoviridae* family, was also enhanced in the cells treated with Mfn2-specific siRNA compared to that in control cells (Fig. 4F).

Given that our knockdown experiments failed to completely deplete Mfn2 protein (the effects were relatively modest), we evaluated IFN-β responses in wild-type (WT) and *Mfn2*-deficient MEFs (*28*). MAVS- and RIG-I–dependent production of IFN-β was significantly enhanced (>4-fold) in the *Mfn2*-deficient cells compared to that of WT cells (Fig. 5A). In addition, reintroduction of Myc-tagged murine Mfn2, but not that of its homolog mMfn1, fully restored suppression of IFN-β production in MEFs from $Mfn2^{-/-}$ mice (Fig. 5B), underscoring the importance of endogenous Mfn2 for the modulation of MAVS-mediated antiviral responses. When the $Mfn2^{-/-}$ MEFs were infected with a recombinant vesicular stomatitis virus (VSV) expressing green fluorescent protein (GFP) (VSVΔG*-G) (*29*), the production of IFN-β protein was substantially increased relative to that of infected WT and *Mfn1*-deficient MEFs (Fig. 5C), and the number of cells expressing GFP was significantly reduced only in the *Mfn2*-deficient MEFs, indicating their increased resistance to VSV infection (Fig. 5D). Furthermore, induction of IFN-β production by a positive-stranded RNA virus of the *Picornavirus* family, encephalomyocarditis virus (EMCV), was also greater in the *Mfn2*-deficient MEFs relative to that of WT MEFs (Fig. 5E), consistent with a role for Mfn2 as an inhibitor of the MAVS-mediated antiviral response.

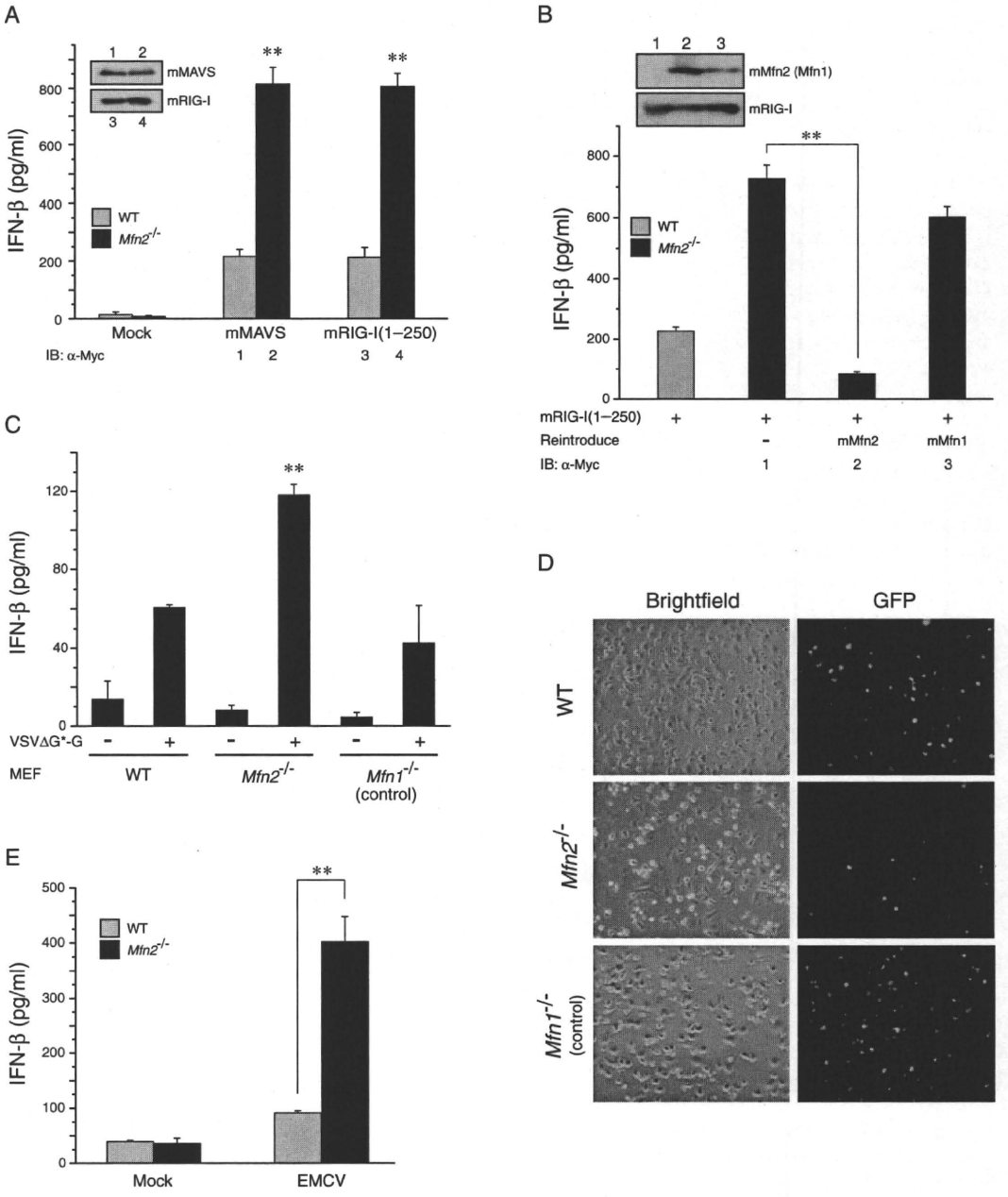

Fig. 5. The effect of Mfn2 deficiency on viral infection in MEFs. (**A**) WT and *Mfn2*-deficient MEFs were transfected with plasmids encoding either murine MAVS or mRIG-I(1–250), and the production of IFN-β was measured by ELISA 24 hours after transfection. Mock treatment of MEFs involved their transfection with equivalent amounts of pcDNA3.1(–). (**B**) Reconstitution of *Mfn2*-deficient MEFs with Mfn2 restores modulation of the IFN-β response. *Mfn2*-deficient MEFs were transfected with plasmids encoding mRIG-I(1–250) and either Myc-tagged mMfn2 or mMfn1, and culture supernatants were harvested 24 hours later for measurement of IFN-β production by ELISA. Expression of the plasmids encoding Mfn2 or Mfn1 was confirmed by analysis of Western blots with an antibody against Myc (inset, lanes 2 and 3). (**C**) This experiment was performed similarly to that described in (A) except that WT and *Mfn2*-deficient MEFs were infected with VSVΔG*-G at an MOI of 3. In this experiment, $Mfn1^{-/-}$ MEFs were also used as a control to evaluate the specificity of Mfn2 in modulating the antiviral response. (**D**) Fluorescence microscopy (GFP) of MEFs infected with VSVΔG*-G at an MOI of 3 for 24 hours. (**E**) WT and *Mfn2*-deficient MEFs were infected with EMCV at an MOI of 3, and the production of IFN-β was measured by ELISA. All ELISA data shown represent mean values ± SD ($n = 3$ experiments). $^{**}P < 0.01$.

The HR1 region of Mfn2 is critical for its interaction with MAVS

Through a coimmunoprecipitation approach, we mapped the region of Mfn2 that interacted with MAVS to a central 4,3 hydrophobic heptad repeat (HR1) region (Mfn2-HR1) (Fig. 6A). An analogous approach with deletion mutants of MAVS yielded results indicating that the C-terminal regions of MAVS (amino acid residues 201 to 540) were both necessary and sufficient for the interaction with Mfn2-HR1, and that both the CARD, which is important for the interaction between MAVS and cytoplasmic RNA helicases, and the proline-rich domain were dispensable for this interaction (Fig. 6B). The interaction between Mfn2-HR1 and MAVS was observed only with the transmembrane-anchored form of MAVS (C-term/TM), indicating that the Mfn2-HR1 fragment recognized a structural or topological element (or both) that was specific to the mitochondrial outer membrane–bound form of MAVS.

These results prompted us to investigate the functional role of the HR1 region in the regulation of the antiviral response. In HEK 293 cells, expression of a plasmid encoding the Mfn2-HR1 fragment potently and dose-dependently suppressed IFN-β and NF-κB responses to the overexpression of MAVS-, RIG-I(1–250), and MDA-5 (Fig. 6C and fig. S4) in a manner similar to that observed with full-length Mfn2, indicating that the HR1 region could behave as a dominant-negative modulator of antiviral signaling. Mutations of the predicted *f* position in the HR1 region (E424G and R468H) (fig. S5), which is exposed on the surface of the protein, resulted in a severe loss of function when we evaluated the ability of the mutated protein to modulate the RIG-I–induced IFN-β response, whereas a GTPase mutant of Mfn2 ($Mfn2^{K109A}$) behaved nearly similarly to WT Mfn2 (Fig. 6D). Although the HR1 region has been characterized as an im-

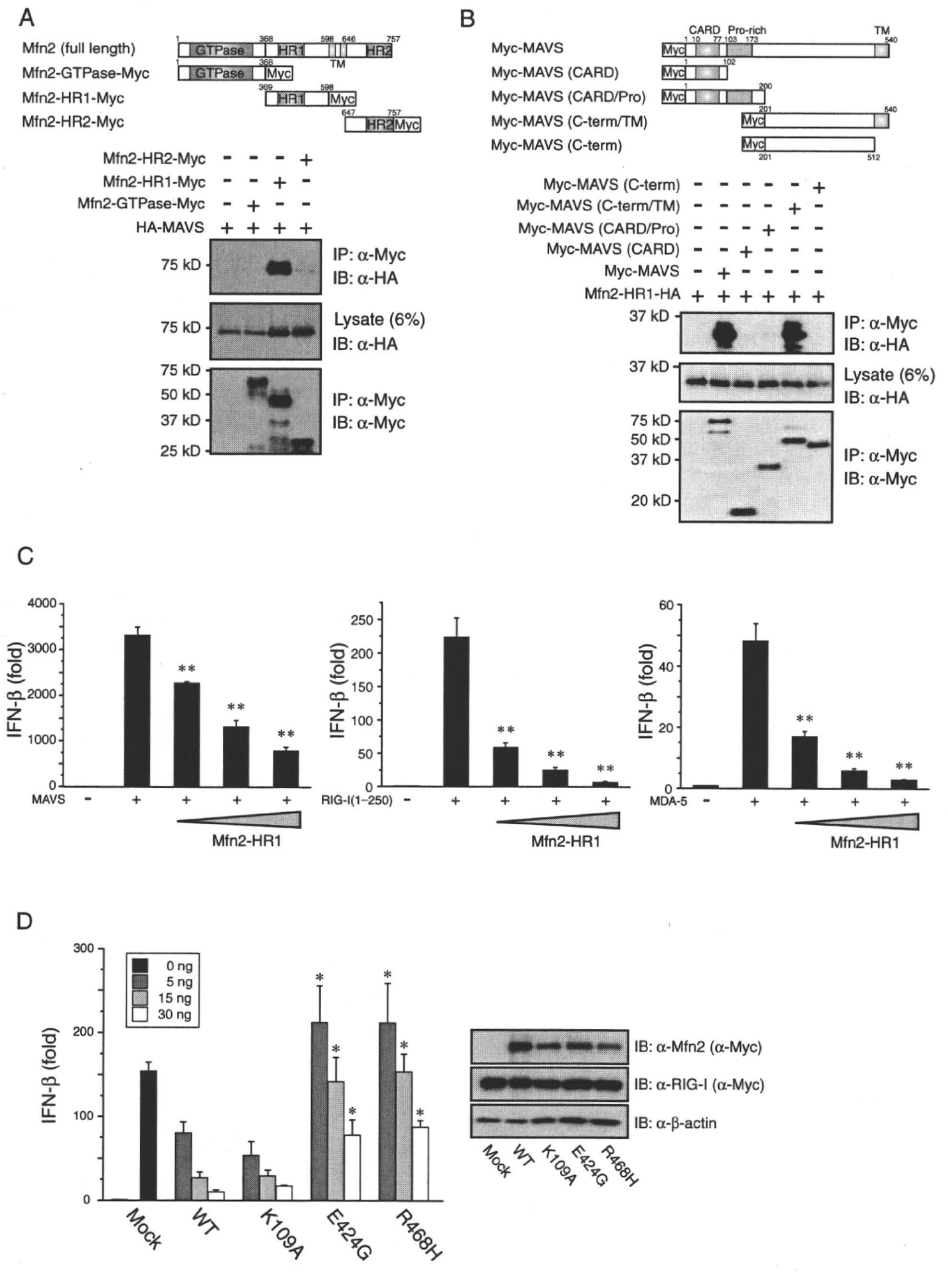

Fig. 6. The HR1 region of Mfn2 associates with MAVS and inhibits activation of the IFN-β reporter. (**A**) Interaction of HA-tagged MAVS and Myc-tagged Mfn2 variants (upper panel) was analyzed by coimmunoprecipitation assays, which were performed as described for Fig. 1B. The GTPase domain, hydrophobic heptad repeats (HR) 1 and 2, and transmembrane segment (TM) are depicted. (**B**) Interaction of truncated MAVS variants with the Mfn2-HR1 fragment. (**C**) HEK 293 cells were cotransfected with 50 ng of plasmids encoding either MAVS, RIG-I(1–250), or MDA-5 together with increasing amounts (20, 50, and 100 ng) of a plasmid encoding the Mfn2-HR1 fragment and the IFN-β luciferase reporter plasmid as described for Fig. 2. (**D**) HEK 293 cells were cotransfected with 50 ng of plasmid encoding RIG-I(1–250) and increasing amounts (5, 15, and 30 ng; inset) of plasmids encoding WT and mutant Mfn2 proteins together with the IFN-β reporter plasmid. Western blots showing the abundance of the WT and mutant Mfn2 proteins, as well as the abundance of stimulated RIG-I(1–250). All data shown represent mean values ± SD (n = 3 experiments). $^{*}P < 0.05$; $^{**}P < 0.01$.

portant domain for mitochondrial targeting (*30*) or fusion (*31*), its functional role in mitofusin homologs is still poorly understood. Our results indicate that the HR1 region of Mfn2 is critical for regulating the antiviral signaling pathway.

Mfn2 functions upstream of TRAF6 and TBK-1

Because Mfn2 was required for regulating antiviral signaling through MAVS, it was likely that Mfn2 acted downstream of (or at the same level as) MAVS in this pathway. In the course of examining the mechanism of its inhibitory activity, we found that Mfn2-specific siRNA had no effect either on the activation of the NF-κB reporter in response to tumor necrosis factor receptor-associated factor 6 (TRAF6) (Fig. 7A), an essential upstream regulator of the inhibitor of κB kinase complex, or on the activation of the IFN-β reporter in response to TANK-binding kinase 1 (TBK-1) (Fig. 7A), a kinase that targets IRF-3, even though both of these effectors act downstream of MAVS (*9*, *15*, *32*, *33*). Consistent with these findings, the production of the proinflammatory cytokine interleukin-6 (IL-6) by TRAF6 was also unaffected in *Mfn2*-deficient MEFs (Fig. 7B), suggesting that Mfn2 inhibited the RIG-I pathway downstream of MAVS and upstream of both TRAF6 (the NF-κB activation pathway) and TBK-1 (the IRF-3 activation pathway).

DISCUSSION

The mitochondrion is well known as the powerhouse of eukaryotic cells, and it is additionally involved in antiviral immunity in vertebrates (*9*–*13*). Despite the central role that the mitochondrial integral membrane protein MAVS plays in this pathway, few additional mitochondrial membrane proteins have been implicated in regulating its activity. In this study, we described our findings that Mfn2, a known mediator of mitochondrial fusion, interacted with MAVS to inhibit antiviral signaling pathways.

Our results show that MAVS forms a stable supramolecular assembly on the outer mitochondrial membrane at physiological pH. We propose that the MAVS complex is an Mfn2-dependent complex because knockdown of endogenous Mfn2 reduced the apparent molecular mass of MAVS, as determined by analytical size exclusion chromatography, from ~600 kD to a lower molecular mass (Fig. 4A). Because loss of endogenous Mfn2 also enhanced the MAVS-mediated antiviral response, it is possible that rearrangement of MAVS from a higher- to a lower-order complex is a prerequisite for the activation of MAVS in response to upstream signaling from RIG-I or MDA-5. Such a model would suggest that Mfn2 functions by stably sequestering MAVS in nonproductive higher-order complexes that are incapable of propagating a downstream antiviral response. A small portion of MAVS did not colocalize with Mfn2, as observed by both size exclusion chromatography (Fig. 4A) and immunofluorescence microscopy (Fig. 1D), raising the possibility that this fraction represents an available pool of MAVS that could be easily activated on viral infection. At present, it is unclear whether the lower-order state is more favorable for recruiting downstream molecules such as TRAF family members or whether it is preferentially competent for signaling to the IRF-3 or NF-κB activation pathways.

In conclusion, we propose a mechanism for the regulation of the cellular antiviral response in which signaling events at the mitochondrial outer membrane involving MAVS are modulated by Mfn2 through its HR1

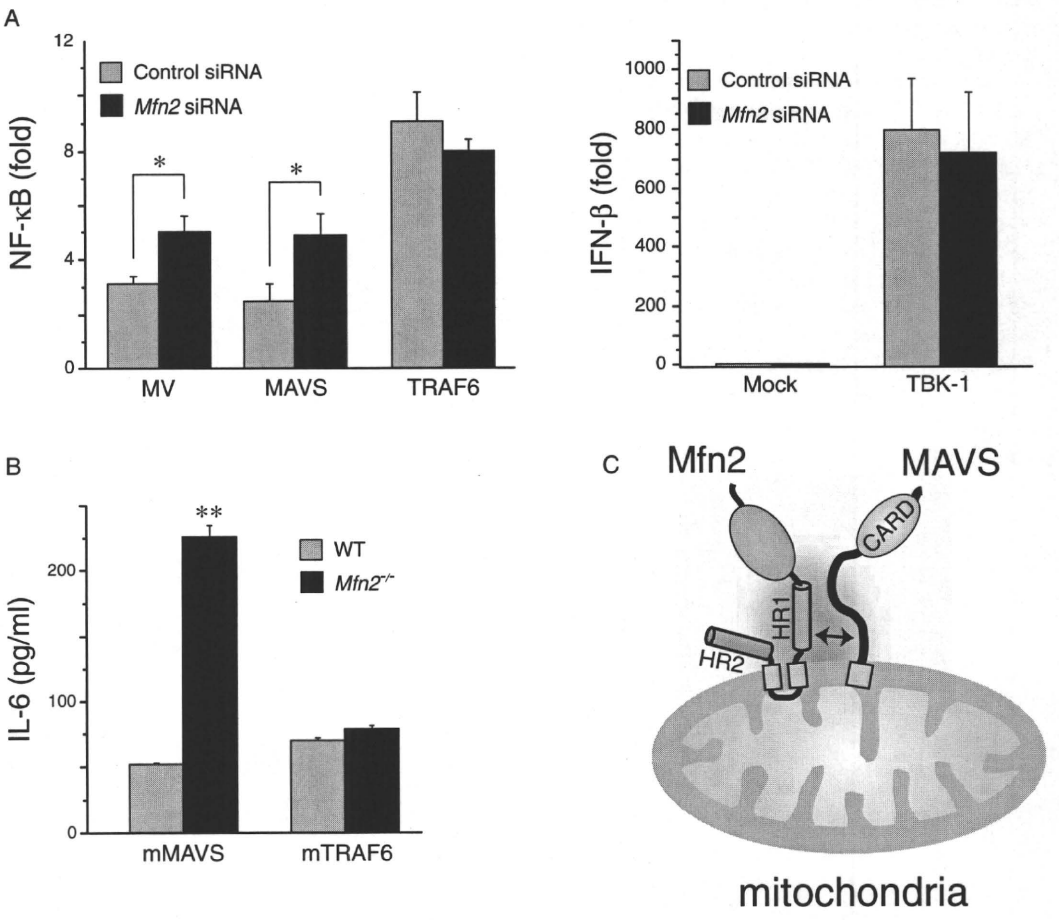

Fig. 7. The role of Mfn2 in antiviral signaling. (**A**) Activation of NF-κB (left panel) and IFN-β (right panel) reporters in siRNA-treated HEK 293 cells transfected with plasmids encoding MAVS, TRAF6, or TBK-1. In the control (left panel), cells were infected with measles virus (MV) at an MOI of 2. (**B**) WT and *Mfn2*-deficient MEFs were transfected with plasmids encoding either mMAVS or mTRAF6, and the subsequent production of IL-6 was measured by ELISA. All data shown represent mean values ± SD (n = 3 experiments). *$P < 0.05$; **$P < 0.01$. (**C**) Schematic representation of the MAVS-Mfn2 interaction on the mitochondrial outer membrane.

region (Fig. 7C) upon formation of a supramolecular complex. In this model, we speculate that Mfn2 inhibits the function of the C-terminal region (including the transmembrane domain) of MAVS rather than blocks its CARD, in contrast to previous findings with NOD-like receptor (NLR) family member X1 (NLRX1), a member of the cytoplasmic NLR family that also modulates MAVS-dependent antiviral signaling (*11*). Moreover, it is noteworthy that inhibition of MAVS-mediated antiviral signaling was not observed with Mfn1, which suggests that Mfn1 and Mfn2 are not functionally redundant and illustrates that Mfn2 has multiple specialized functions in the cell (*22–24*, *34*). A small amount of Mfn2 is thought to be present in the ER (*22*). In addition, stimulator of interferon genes (STING) [also termed MITA (*13*)], an essential mediator of the activation of IRF-3, is also present in the ER, mitochondria, or both and interacts with MAVS (*35*). Collectively, these findings raise questions about the interplay between the ER and mitochondria that control antiviral signaling and raise the possibility that Mfn2 may be involved.

MATERIALS AND METHODS

Cell culture

The HEK 293 and HeLa cell lines were maintained in Dulbecco's modified Eagle's medium (DMEM, GIBCO BRL) supplemented with 1% L-glutamine, 1% penicillin-streptomycin, and 10% bovine calf serum or 10% fetal calf serum, respectively, at 5% CO_2 and 37°C. WT, *Mfn1*$^{-/-}$, and *Mfn2*$^{-/-}$ MEFs were provided by D. Chan (Howard Hughes Medical Institute, Caltech) and maintained in standard medium (DMEM supplemented with 10% bovine calf serum) as described previously (*28*). Immunofluorescence microscopy to visualize mitochondria was performed as described previously (*19*, *28*).

Plasmid constructions and mutagenesis

Total messenger RNA (mRNA) from HEK 293 and MEFs was isolated with the TRIzol reagent (Invitrogen) and reverse-transcribed with moloney murine leukemia virus reverse transcriptase (Wako Pure Chemical Industries, Tokyo, Japan). Polymerase chain reaction assays were performed with PrimeSTAR DNA polymerase (Takara, Tokyo, Japan). The following primers (see Supplementary Materials for sequences) were used to generate the complete open reading frames of human MAVS: TK349/TK356; hMfn2: TK365/TK366; hMfn1: TK363/TK364; hFis1: TK367/TK368; hRIG-I(1–250): TK357/TK358; hMDA-5: TK442/TK443; hTBK-1: TK497/TK498; murine MAVS: TK300/TK307; and mRIG-I(1–250): TK310/TK345. Plasmids encoding epitope-tagged MAVS proteins were constructed by ligating the MAVS cDNA into Not I– and Eco RV–digested pcDNA3.1(−) vector (Invitrogen) that encoded either an N-terminal 3× Myc or 3× hemagglutinin (HA) tag. The hMfn2, hMfn1, hRIG-I(1–250), and hMDA-5 cDNAs were ligated into pcDNA3.1 that encoded either a C-terminal 7× Myc or a 3× HA tag.

Antibodies

Antibodies against human MAVS (hMAVS) and murine MAVS (mMAVS) were generated by immunizing rabbits with either recombinant N-terminal histidine-tagged hMAVS (amino acid residues 1 to 175) or mMAVS (amino acid residues 1 to 173), respectively. The recombinant proteins were overexpressed in *Escherichia coli* and purified from solubilized inclusion bodies. The immunoglobulin G (IgG) fractions were affinity-purified with the Econo-Pac Protein A Kit (BioRad). Monoclonal antibodies against Myc (9E10) and HA (HA.11) were purchased from Covance. Monoclonal antibodies against hMfn2, hTom20, IRF-3, and β-actin were obtained from Santa Cruz, and the rabbit monoclonal antibody (4D4G) against phosphorylated IRF-3 (at Ser^{396}) was from Cell Signaling. The Alexa Fluor 568–conjugated monoclonal antibody against mouse IgG was purchased from Molecular Probes. Polyclonal antibody against hFis1 was from ALEXIS Biochemicals. The monoclonal antibody against mitochondrial heat shock protein 70 (mtHsp70) was from Affinity BioReagents. The polyclonal antibody against rat Mfn2 was a gift from K. Mihara (Kyushu University, Japan).

Analytical size exclusion chromatography

Three 10-cm dishes of confluent HEK 293 cells were washed once with cold 1× phosphate-buffered saline (PBS) (pH 7.2), and cells were scraped off and lysed in 1 ml of homogenization buffer [20 mM Hepes (pH 7.5), 70 mM sucrose, and 220 mM mannitol] by 30 strokes in a Dounce homogenizer. The homogenate was centrifuged at 800*g* for 5 min to precipitate nuclei, and the resulting supernatant was further centrifuged at 10,000*g* for 10 min at 4°C to precipitate the crude mitochondrial fraction. After the pellet was washed once with homogenization buffer, the mitochondrial extracts were prepared by solubilization with lysis buffer [50 mM tris-HCl (pH 7.2), 200 mM NaCl, 10% glycerol, and 1% digitonin] and clarification by centrifugation at 12,000*g* for 5 min. Size exclusion chromatography of mitochondrial extracts was performed on Superdex-200 HR-10/30 or Superose 6 HR-10/30 columns (GE Healthcare) equilibrated with 50 mM tris-HCl (pH 7.2) containing 200 mM NaCl, 10% glycerol, and 0.1% NP-40. Extracts were loaded onto the column at a flow rate of 0.3 ml/min at room temperature. Fractions (600 μl each) were collected, resolved by 8% SDS–polyacrylamide gel electrophoresis (SDS-PAGE), and analyzed by Western blotting with either a polyclonal antibody against hMAVS (see above) or a monoclonal antibody against hMfn2. For the analysis of Fis1, fractions were resolved by 15% SDS-PAGE followed by Western blotting analysis with a polyclonal antibody against hFis1. The following molecular weight standards (GE Healthcare) were used: Blue Dextran-2000 (2000 kD), thyroglobulin (669 kD), ferritin (440 kD), catalase (232 kD), and bovine serum albumin (67 kD).

Immunoprecipitation of the hMAVS complex

HEK 293 cells were transfected with the expression plasmid encoding 3× Myc-tagged hMAVS (see above) by the calcium phosphate method. Transfected cells were selected in DMEM medium supplemented with hygromycin B (200 μg/ml; Wako Pure Chemical Industries) for 2 weeks. Stably transfected cells were grown to confluence on five 15-cm dishes. Cells were washed three times with 1× PBS (pH 7.2) and lysed with 10 ml of lysis buffer [20 mM Hepes (pH 7.5), 150 mM NaCl, 10% glycerol, 1 mM EDTA, 1 mM DTT, and 1% digitonin] supplemented with Complete Mini Protease Inhibitor Cocktail (Roche). The clarified supernatant was incubated with monoclonal antibody against the Myc tag (9E10) at 4°C for 2 hours, after which 60 μl of protein A–Sepharose beads (GE Healthcare) was added. After incubation for 5 hours at 4°C, the beads were washed three times with lysis buffer, and immunoprecipitates were resolved by 10% SDS-PAGE. Silver-stained bands were analyzed by LC/MS/MS (Medical Institute of Bioregulation, Kyushu University, Japan).

Coimmunoprecipitations

Coimmunoprecipitation experiments were performed as described previously (*36*) with minor modifications. HEK 293 cells at 80% confluence were transiently transfected with the appropriate plasmids (2 μg each) in a six-well plate by the calcium phosphate method. Two days after transfection, cells were lysed with 1 ml of lysis buffer [50 mM tris-HCl (pH 7.4), 150 mM NaCl, 10% glycerol, and 1% NP-40], and the clarified supernatants were incubated overnight at 4°C with 20 μl of agarose beads (Sigma-Aldrich) conjugated to a polyclonal antibody against *c*-Myc. After four washes with 1× PBS (pH 7.2), immunoprecipitates were resolved by 8 or 12% SDS-PAGE and analyzed by Western blotting with a monoclonal antibody (HA.11) against the HA tag followed by a horseradish peroxidase (HRP)-conjugated antibody against mouse IgG (Jackson ImmunoResearch). To immunoprecipitate endogenous MAVS, HEK 293 cells and MEFs were

lysed with 1% digitonin lysis buffer, and the clarified supernatants were incubated with 10 μg of antibody against hMAVS or mMAVS, followed by incubation overnight at 4°C with 20 μl of protein A–Sepharose beads. The beads were washed four times with lysis buffer, and immunoprecipitates were resolved by 8% SDS-PAGE, analyzed by Western blotting with a monoclonal antibody against hMfn2, and detected with a HRP-conjugated antibody against mouse IgG.

Luciferase assays

HEK 293 cells (2×10^5 cells per well) were plated in 24-well plates. The following day, cells were cotransfected with 100 ng of a luciferase reporter plasmid (p125luc or pELAM), 2.5 ng of the *Renilla* luciferase internal control vector phRL-TK (Promega), and each of the indicated plasmids with the Lipofectamine 2000 reagent (Invitrogen). Empty vector [pcDNA3.1(−)] was used to maintain equivalent amounts of DNA in each well. Cells were harvested 24 hours after transfection and analyzed by a dual-luciferase reporter assay on the GloMax 20/20n luminometer (Promega). Each experiment was replicated at least three times. The p125luc reporter plasmid was provided by T. Taniguchi (University of Tokyo, Japan).

Native PAGE

Native PAGE experiments were performed as described previously (*37*).

RNA interference

For RNA interference–based knockdown experiments, a 25-nucleotide siRNA was purchased from Invitrogen (Stealth Select RNAi). HEK 293 cells were transfected with 50 nM siRNA (final concentration) with Lipofectamine RNAiMAX (Invitrogen). The following day, cells were transfected with luciferase reporter plasmids and then harvested after an additional 24 hours. The designation and sequence (sense strand only) of the Stealth Select RNAi oligonucleotides used in the study were hMfn2 (HSS115028) and 5′-ggaccuccaugggcauucuuguugu-3′, respectively. Stealth RNAi Negative Control Medium GC Duplex #2 (Invitrogen) was used as the control.

ELISA

Production of IFN-β by HEK 293 cells and MEFs was measured with species-specific ELISA reagents for human and murine IFN-β from Kamakura Techno-Science Inc. (Kanagawa, Japan) and PBL Biomedical Laboratories, respectively. The ELISA kit for murine IL-6 was purchased from R&D Systems.

Viral infections

The siRNA-treated HEK 293 cells, which were also cotransfected with reporter plasmids, were plated in 12-well plates and incubated overnight. When the cells were 50% confluent, the culture medium was aspirated and the cells were infected with 200 μl of the Edmonston strain of measles virus (*38*) at 37°C at a multiplicity of infection (MOI) of 2. One hour after infection, cells were supplemented with 800 μl of standard DMEM, then incubated for another 48 hours before the performance of luciferase assays. MEFs were infected with either VSVΔG*-G (*29*) or EMCV (*25*) at an MOI of 3 and incubated for 24 hours before analysis by ELISA, as described above.

SUPPLEMENTARY MATERIALS

www.sciencesignaling.org/cgi/content/full/2/84/ra47/DC1

Materials

Fig. S1. Interaction between endogenous mMfn2 and mMAVS in MEFs.

Fig. S2. Knockdown of Mfn2 with specific siRNA results in enhanced MAVS-mediated activation of the IFN-β reporter.

Fig. S3. Treatment of HEK 293 cells with Mfn2-specific siRNA increased the production of endogenous IFN-β in response to transfection with poly(I:C).

Fig. S4. Mfn2-HR1 is a dominant-negative modulator of MAVS-mediated activation of NF-κB.

Fig. S5. Sequence alignment of Mfn2 homologs within HR1.

Table S1. List of mitochondrial proteins, other than Mfn2, that were identified by LC/MS/MS.

Reference

REFERENCES AND NOTES

1. J. A. Hoffmann, F. C. Kafatos, C. A. Janeway Jr., R. A. B. Ezekowitz, Phylogenetic perspectives in innate immunity. *Science* **284**, 1313–1318 (1999).
2. S. Akira, K. Takeda, T. Kaisho, Toll-like receptors: Critical proteins linking innate and acquired immunity. *Nat. Immunol.* **2**, 675–680 (2001).
3. T. Kawai, S. Akira, Innate immune recognition of viral infection. *Nat. Immunol.* **7**, 131–137 (2006).
4. A. Le Bon, D. F. Tough, Links between innate and adaptive immunity via type I interferon. *Curr. Opin. Immunol.* **14**, 432–436 (2002).
5. A. Iwasaki, R. Medzhitov, Toll-like receptor control of the adaptive immune responses. *Nat. Immunol.* **5**, 987–995 (2004).
6. X. Wang, The expanding role of mitochondria in apoptosis. *Genes Dev.* **15**, 2922–2933 (2001).
7. S. Raha, B. H. Robinson, Mitochondria, oxygen free radicals, disease and ageing. *Trends Biochem. Sci.* **25**, 502–508 (2000).
8. G. A. Rutter, R. Rizzuto, Regulation of mitochondrial metabolism by ER Ca^{2+} release: An intimate connection. *Trends Biochem. Sci.* **25**, 215–221 (2000).
9. R. B. Seth, L. Sun, C. K. Ea, Z. J. Chen, Identification and characterization of MAVS, a mitochondrial antiviral signaling protein that activates NF-κB and IRF3. *Cell* **122**, 669–682 (2005).
10. X. D. Li, L. Sun, R. B. Seth, G. Pineda, Z. J. Chen, Hepatitis C virus protease NS3/4A cleaves mitochondrial antiviral signaling protein off the mitochondria to evade innate immunity. *Proc. Natl. Acad. Sci. U.S.A.* **102**, 17717–17722 (2005).
11. C. B. Moore, D. T. Bergstralh, J. A. Duncan, Y. Lei, T. E. Morrison, A. G. Zimmermann, M. A. Accavitti-Loper, V. J. Madden, L. Sun, Z. Ye, J. D. Lich, M. T. Heise, Z. Chen, J. P. Ting, NLRX1 is a regulator of mitochondrial antiviral immunity. *Nature* **451**, 573–577 (2008).
12. I. Tattoli, L. A. Carneiro, M. Jéhanno, J. G. Magalhaes, Y. Shu, D. J. Philpott, D. Arnoult, S. E. Girardin, NLRX1 is a mitochondrial NOD-like receptor that amplifies NF-κB and JNK pathways by inducing reactive oxygen species production. *EMBO Rep.* **9**, 293–300 (2008).
13. B. Zhong, Y. Yang, S. Li, Y. Y. Wang, Y. Li, F. Diao, C. Lei, X. He, L. Zhang, P. Tien, H. B. Shu, The adaptor protein MITA links virus-sensing receptors to IRF3 transcription factor activation. *Immunity* **29**, 538–550 (2008).
14. T. Kawai, K. Takahashi, S. Sato, C. Coban, H. Kumar, H. Kato, K. J. Ishii, O. Takeuchi, S. Akira, IPS-1, an adaptor triggering RIG-I- and Mda5-mediated type I interferon induction. *Nat. Immunol.* **6**, 981–988 (2005).
15. L. G. Xu, Y. Y. Wang, K. J. Han, L. Y. Li, Z. Zhai, H. B. Shu, VISA is an adapter protein required for virus-triggered IFN-β signaling. *Mol. Cell* **19**, 727–740 (2005).
16. E. Meylan, J. Curran, K. Hofmann, D. Moradpour, M. Binder, R. Bartenschlager, J. Tschopp, Cardif is an adaptor protein in the RIG-I antiviral pathway and is targeted by hepatitis C virus. *Nature* **437**, 1167–1172 (2005).
17. H. Kumar, T. Kawai, H. Kato, S. Sato, K. Takahashi, C. Coban, M. Yamamoto, S. Uematsu, K. J. Ishii, O. Takeuchi, S. Akira, Essential role of IPS-1 in innate immune responses against RNA viruses. *J. Exp. Med.* **203**, 1795–1803 (2006).
18. Q. Sun, L. Sun, H. H. Liu, X. Chen, R. B. Seth, J. Forman, Z. J. Chen, The specific and essential role of MAVS in antiviral innate immune responses. *Immunity* **24**, 633–642 (2006).
19. A. Jofuku, N. Ishihara, K. Mihara, Analysis of functional domains of rat mitochondrial Fis1, the mitochondrial fission-stimulating protein. *Biochem. Biophys. Res. Commun.* **333**, 650–659 (2005).
20. D. C. Chan, Mitochondrial fusion and fission in mammals. *Annu. Rev. Cell Dev. Biol.* **22**, 79–99 (2006).
21. A. Santel, S. Frank, B. Gaume, M. Herrler, R. J. Youle, M. T. Fuller, Mitofusin-1 protein is a generally expressed mediator of mitochondrial fusion in mammalian cells. *J. Cell Sci.* **116**, 2763–2774 (2003).
22. O. M. de Brito, L. Scorrano, Mitofusin 2 tethers endoplasmic reticulum to mitochondria. *Nature* **456**, 605–610 (2008).
23. K. H. Chen, X. Guo, D. Ma, Y. Guo, Q. Li, D. Yang, P. Li, X. Qiu, S. Wen, R. P. Xiao, J. Tang, Dysregulation of HSG triggers vascular proliferative disorders. *Nat. Cell Biol.* **6**, 872–883 (2004).
24. S. Züchner, I. V. Mersiyanova, M. Muglia, N. Bissar-Tadmouri, J. Rochelle, E. L. Dadali, M. Zappia, E. Nelis, A. Patitucci, J. Senderek, Y. Parman, O. Evgrafov, P. D. Jonghe, Y. Takahashi, S. Tsuji, M. A. Pericak-Vance, A. Quattrone, E. Battologlu, A. V. Polyakov, V. Timmerman, J. M. Schröder, J. M. Vance, Mutations in the mitochondrial GTPase mitofusin 2 cause Charcot-Marie-Tooth neuropathy type 2A. *Nat. Genet.* **36**, 449–451 (2004).

25. M. Yoneyama, M. Kikuchi, T. Natsukawa, N. Shinobu, T. Imaizumi, M. Miyagishi, K. Taira, S. Akira, T. Fujita, The RNA helicase RIG-I has an essential function in double- stranded RNA-induced innate antiviral responses. *Nat. Immunol.* **5**, 730–737 (2004).
26. L. Gitlin, W. Barchet, S. Gilfillan, M. Cella, B. Beutler, R. A. Flavell, M. S. Diamond, M. Colonna, Essential role of mda-5 in type I IFN responses to polyriboinosinic: Polyribocytidylic acid and encephalomyocarditis picornavirus. *Proc. Natl. Acad. Sci. U.S.A.* **103**, 8459–8464 (2006).
27. H. Kato, O. Takeuchi, S. Sato, M. Yoneyama, M. Yamamoto, K. Matsui, S. Uematsu, A. Jung, T. Kawai, K. J. Ishii, O. Yamaguchi, K. Otsu, T. Tsujimura, C. S. Koh, C. Reis e Sousa, Y. Matsuura, T. Fujita, S. Akira, Differential roles of MDA5 and RIG-I helicases in the recognition of RNA viruses. *Nature* **441**, 101–105 (2006).
28. H. Chen, S. A. Detmer, A. J. Ewald, E. E. Griffin, S. E. Fraser, D. C. Chan, Mitofusins Mfn1 and Mfn2 coordinately regulate mitochondrial fusion and are essential for embryonic development. *J. Cell Biol.* **160**, 189–200 (2003).
29. A. Takada, C. Robison, H. Goto, A. Sanchez, K. G. Murti, M. A. Whitt, Y. Kawaoka, A system for functional analysis of Ebola virus glycoprotein. *Proc. Natl. Acad. Sci. U.S.A.* **94**, 14764–14769 (1997).
30. M. Rojo, F. Legros, D. Chateau, A. Lombès, Membrane topology and mitochondrial targeting of mitofusins, ubiquitous mammalian homologs of the transmembrane GTPase Fzo. *J. Cell Sci.* **115**, 1663–1674 (2002).
31. E. E. Griffin, D. C. Chan, Domain interactions within Fzo1 oligomers are essential for mitochondrial fusion. *J. Biol. Chem.* **281**, 16599–16606 (2006).
32. S. M. McWhirter, B. R. Tenoever, T. Maniatis, Connecting mitochondria and innate immunity. *Cell* **122**, 645–647 (2005).
33. R. Yoshida, G. Takaesu, H. Yoshida, F. Okamoto, T. Yoshioka, Y. Choi, S. Akira, T. Kawai, A. Yoshimura, T. Kobayashi, TRAF6 and MEKK1 play a pivotal role in the RIG-I-like helicase antiviral pathway. *J. Biol. Chem.* **283**, 36211–36220 (2008).
34. S. Pich, D. Bach, P. Briones, M. Liesa, M. Camps, X. Testar, M. Palacin, A. Zorzano, The Charcot-Marie-Tooth type 2A gene product, Mfn2, up-regulates fuel oxidation through expression of OXPHOS system. *Hum. Mol. Genet.* **14**, 1405–1415 (2005).
35. H. Ishikawa, G. N. Barber, STING is an endoplasmic reticulum adaptor that facilitates innate immune signalling. *Nature* **455**, 674–678 (2008).
36. T. Koshiba, S. A. Detmer, J. T. Kaiser, H. Chen, J. M. McCaffery, D. C. Chan, Structural basis of mitochondrial tethering by mitofusin complexes. *Science* **305**, 858–862 (2004).
37. T. Iwamura, M. Yoneyama, K. Yamaguchi, W. Suhara, W. Mori, K. Shiota, Y. Okabe, H. Namiki, T. Fujita, Induction of IRF-3/-7 kinase and NF-κB in response to double-stranded RNA and virus infection: Common and unique pathways. *Genes Cells* **6**, 375–388 (2001).
38. Y. Yanagi, M. Takeda, S. Ohno, Measles virus: Cellular receptors, tropism and pathogenesis. *J. Gen. Virol.* **87**, 2767–2779 (2006).
39. We are grateful to D. Chan (Howard Hughes Medical Institute and California Institute of Technology, Pasadena, CA) for helpful discussions and for providing wild-type, *Mfn1*-, and *Mfn2*-deficient MEF cell lines. We are also grateful to J. Kulman (Puget Sound Blood Center, Seattle, WA) and K. Mihara (Kyushu University, Japan) for their valuable comments on the study. We thank M. Matsumoto and M. Oda (Kyushu University) for the LC/MS/MS analysis, and Y. Fuchigami for technical assistance with DNA sequencing. The p125luc reporter plasmid was provided by T. Taniguchi (University of Tokyo, Japan). We also thank A. Yoshimura and T. Kobayashi (Keio University, Japan) for providing the FLAG-mTRAF6 expression plasmid, and T. Fujita and M. Yoneyama (Kyoto University, Japan) for EMCV. K.Y. was supported by an Academic Challenge grant by Venture Business Laboratory, Kyushu University. This work was supported by the grants-in-aid for Young Scientists (B) from the Ministry of Education, Culture, Sports, Science, and Technology of Japan (20770123), Kyushu University Interdisciplinary Programs in Education and Projects in Research Development (P & P type D; 20301), and The Uehara Memorial Foundation to T.K. The authors declare that they have no conflict of interest.

Submitted 24 February 2009
Accepted 31 July 2009
Final Publication 18 August 2009
10.1126/scisignal.2000287
Citation: K. Yasukawa, H. Oshiumi, M. Takeda, N. Ishihara, Y. Yanagi, T.Seya, S. Kawabata, T. Koshiba, Mitofusin 2 inhibits mitochondrial antiviral signaling. *Sci. Signal.* **2**, ra47 (2009).

European Journal of Immunology

Oligomerized TICAM-1 (TRIF) in the cytoplasm recruits nuclear BS69 to enhance NF-κB activation and type I IFN induction

Hiromi Takaki, Hiroyuki Oshiumi*, Miwa Sasai, Takahiro Kawanishi, Misako Matsumoto and Tsukasa Seya*

Department of Microbiology and Immunology, Graduate School of Medicine, Hokkaido University, Kita-ku, Sapporo, Japan

Although adenovirus 5 E1A-binding protein (BS69) is a nuclear protein acting as a transcriptional repressor, we found by an yeast two-hybrid and human cell immunoprecipitation another cytoplasmic function for this protein. BS69 bound Toll-interleukin 1 receptor domain (TIR)-containing adaptor molecule-1 (TICAM-1) (also named TRIF), an adaptor protein that couples with TLR3 around the endosome. BS69 translocated from the nucleus to the cytoplasm when cells were stimulated with dsRNA or transfected with TICAM-1. Confocal analysis of cells with over-expressed TICAM-1 or those stimulated with dsRNA revealed the characteristic "TICAM-1 speckle", which reflects signalosome formation necessary for the activation of NF-κB and IFN-regulatory factor (IRF)-3. BS69 was involved in the TICAM-1 complex, and the activation of NF-κB/IRF-3 followed by cytokine production was augmented in the presence of BS69 overexpression. Knockdown of endogenous BS69 resulted in a decrease of IFN-β induction, suggesting that BS69 is a positive regulator for the TLR3-TICAM-1 pathway. These results, together with a recent report showing the negative regulatory properties of BS69 in NF-κB activation by EBV-derived latent membrane protein 1, suggest that BS69 harbors dual modes of cytoplasmic NF-κB regulation, positively in the TICAM-1 pathway and negatively in the latent membrane protein 1 pathway.

Key words: BS69 · IFN-β · NF-κB · TICAM-1/TRIF · TLR3

Supporting Information available online

Introduction

Toll-interleukin 1 receptor domain (TIR)-containing adaptor molecule-1 (TICAM-1) acts as an adaptor for TLR3 and activates both the IFN-regulatory factor (IRF)-3 and the IFN-β promoter [1]. TLR3 is localized to the endosome in immature myeloid dendritic cells (mDC) and resting macrophages [2]. Recent imaging analyses revealed that TICAM-1 merges with endosomal TLR3 within 20 min in response to dsRNA stimuli, and after 60 min translocates to form speckles in the cytoplasm which represent the TICAM-1 signalosome [3]. NAP1 and RIP1 are recruited to the TICAM-1 complex, both of which are known to be important factors for activating downstream elements of the TICAM-1 pathway [3, 4]. The forced expression of TICAM-1 leads to the formation of multimers in the signalosome complex [4]. To elucidate what molecules constitute the TICAM-1 complex, we screened TICAM-1-binding proteins by

Correspondence: Dr. Tsukasa Seya
e-mail: seya-tu@pop.med.hokudai.ac.jp

*These authors contributed equally to this work.

an yeast two-hybrid assay. We identified adenovirus 5 E1A-binding protein (BS69) as a member of the TICAM-1 signalosome, in addition to the TRAF family proteins previously noted [1].

BS69, a multidomain cellular protein containing PHD, Bromo, PWWP and MYND domains [5], was originally identified as an adenovirus E1A-binding protein that inhibits the transactivation function of E1A [6, 7]. The C-terminal MYND domain of BS69 was shown to bind to the PxLxP motif existing on E1A, EBV-encoded EBNA2 and a Myc-related cellular protein MGA [8]. Although BS69 is unequivocally a nuclear protein, it has been shown that BS69 interacts with EBV-encoded latent membrane protein 1 (LMP1) in the cytoplasm through its MYND domain and acts as a scaffold protein in the LMP1-mediated JNK pathway by interacting with TRAF6 [9]. Furthermore, a recent report speculated that nuclear BS69 colocalizes with LMP1 in the cytoplasm proximal to the nucleus [10]. The stimulus which induces BS69 protein trafficking, however, remains undetermined.

In this study, we identified BS69 as a TICAM-1-binding protein and demonstrated that the TLR3 agonist polyI:C facilitates the BS69 nucleus-to-cytoplasm trafficking. This property of BS69 further highlights the function of this protein in the cytoplasm: BS69 is involved in the TICAM-1 complex and participates in TICAM-1-mediated IRF-3 and NF-κB activation. Here, we clarified a trigger of BS69 movement and the function of BS69 in the TICAM-1 pathway.

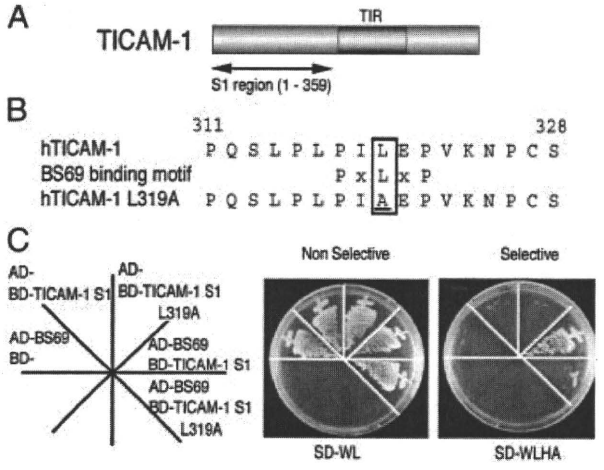

Figure 1. Yeast two-hybrid screening for the collection of TICAM-1-binding proteins. (A) The schema of human TICAM-1 protein. The S1 region (1–359 aa) of TICAM-1 was inserted into the pGBKT7 (bait) vector. From a total of 2.2 billion genes, six genes were obtained which encode for gene products capable of binding to the TICAM-1-S1 region. (B) Sequence alignment of human TICAM-1 and the BS69-binding motif (PxLxP). A point mutation (L319A) was introduced into the PxLxP motif. (C) Interaction between TICAM-1 S1 and BS69 in the yeast two-hybrid system. A strong association was observed between TICAM-1 S1 and BS69 (SD-WLHA plate), whereas the TICAM-1 S1 L319A-BS69 association was barely observable in the SD-WLHA plate.

Results

Yeast two-hybrid screening for collection of TICAM-1-binding proteins

TICAM-1 is a 712 aa protein (Fig. 1A). Since high background expression disturbed screening with the full-length protein, two segments consisting of the N-terminal S1 (1–359 aa) and C-terminal S2 (368-712 aa) regions were separately expressed in yeast (Fig. 1A). No growth was observed in yeast expressing solely S1 (Fig. 1C). The S1 and S2 fragments were ligated into pGBD-C1 and pGBKT7, respectively, to act as bait plasmids. The yeast cells containing bait plasmids were cultured on SD medium lacking Trp, Leu and His, while those cells harboring prey plasmids containing a human lung cDNA library were cultured on SD medium without Trp, Leu, His and Ade. Positive colonies were harvested and retested in the same growth medium (Fig. 1C). Six genes were finally obtained which encoded for gene products responsible for the S1 binding (data not shown). BS69 as well as TRAF-1, TRAF-2 and TRAF-6 were identified as TICAM-1-binding molecules. A reported BS69-binding motif, PxLxP, was identified in the 317–321 aa portion of TICAM-1 (Fig. 1B).

BS69 as a TICAM-1 N-terminal-binding protein

The direct binding of BS69 to the N-terminal of TICAM-1 was confirmed by retesting in yeast. We found the PxLxP motif at 317–321 aa in the TICAM-1 S1 fragment was crucial for BS69 binding, since a TICAM-1 S1 mutant (mt) containing a single point mutation (L319A) resulting in PxAxP, failed to bind BS69 (Fig. 1C). Next, plasmids with the BS69 cDNA and TICAM-1 cDNA were transfected into HEK293 cells and immunoprecipitation was performed. As observed in the yeast cells, WT TICAM-1 coprecipitated with BS69 (Fig. 2A). When the PxLxP motif in the N-terminal region of TICAM-1 was mutated to PxAxP, no BS69 binding was observed (data not shown). Hence, the mt lost the ability to bind BS69 in human cells as well as yeast, indicating that BS69 directly binds the PxLxP motif in the TICAM-1 molecule.

The interaction between TICAM-1 and BS69 was further examined in human cells by molecular imaging. When WT TICAM-1 was co-expressed with BS69 in HeLa cells, the majority of cells showed typical speckle-like TICAM-1 expression (Fig. 2B). This is consistent with a previous report [4], although ~30% of the cells displayed a diffuse expression profile of TICAM-1 (Fig. 2C). BS69 was exclusively stained in the nucleus in cells with diffuse TICAM-1 expression. Surprisingly, in cells with speckled TICAM-1, the cytoplasmic TICAM-1 merged with BS69 by FLAG tag staining. The results indicate that BS69 translocates from the nucleus to the cytoplasm by TICAM-1 over-expression and binds speckled TICAM-1 in the cytoplasm.

The TICAM-1 RHIM mt is efficiently expressed in cells without the induction of apoptosis [3], whereas TICAM-1 N+TIR P434H lacks the two sites essential for self-oligomerization [4]. We found that BS69 recruitment by TICAM-1 occurs in parallel with TICAM-1 oligomerization (speckle formation), since the RHIM mt

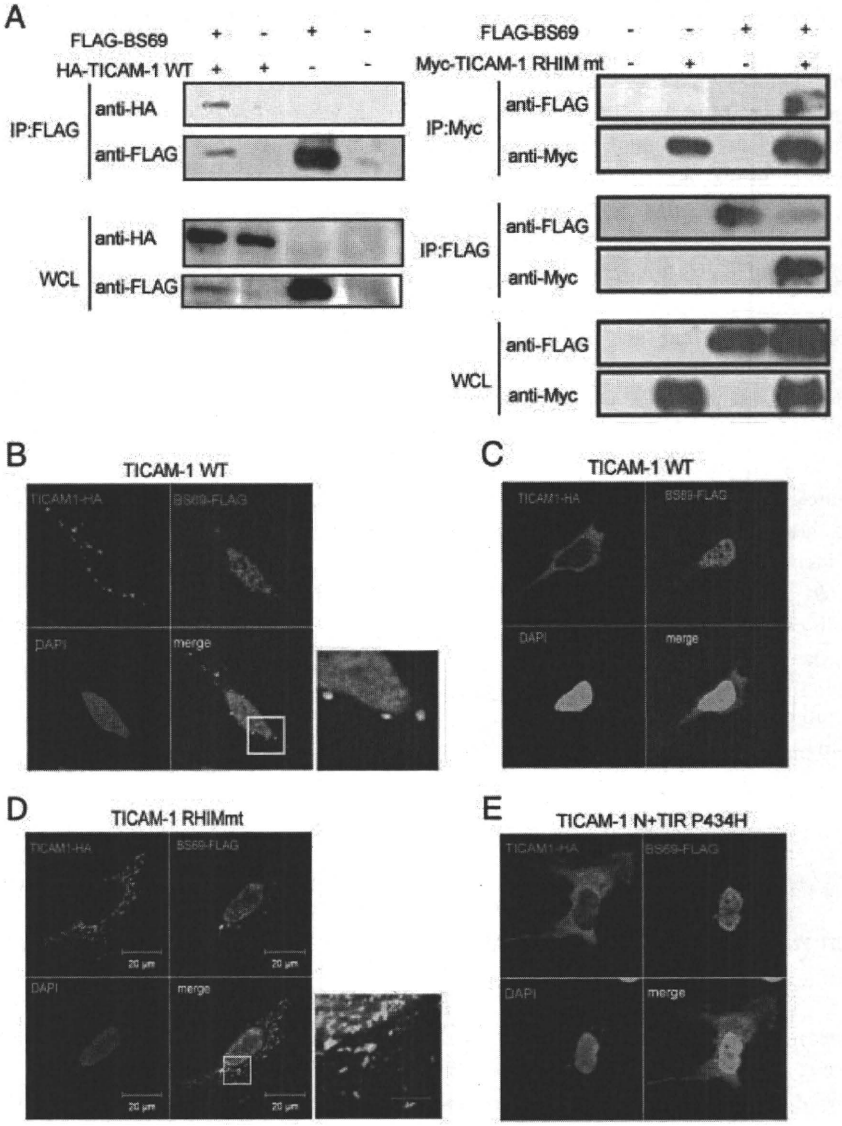

Figure 2. BS69 co-localizes with activated TICAM-1. (A) *Left panel*, HEK 293T cells were transfected with pEF-BOS HA-TICAM-1 WT and pEF-BOS FLAG-BS69. After 24 h, the cells were lysed, immunoprecipitated with anti-FLAG Ab and immunoblotted with anti-HA or anti-FLAG Ab. An aliquot of each whole cell lysate (WCL) was immunoblotted with either anti-HA or anti-FLAG Ab. A typical speckle pattern of TICAM-1 was observed. *Right panel*, HEK 293T cells were transfected with pEF-BOS Myc-TICAM-1 RHIM mt and pEF-BOS FLAG BS69. After 24 h, the cells were lysed, immunoprecipitated with anti-FLAG or anti-Myc Ab and immunoblotted with anti-Myc or anti-FLAG Ab. An aliquot of each whole cell lysate (WCL) was immunoblotted with either anti-Myc or anti-FLAG Ab. (B and C) HeLa cells were transfected with 1 ng of pEF-BOS HA-human TICAM-1 WT and 400 ng of pEF-BOS FLAG-human BS69. After 24 h, the cells were fixed and stained with anti-HA and anti-FLAG Ab, and visualized with either Alexa Fluor 488- or Alexa Fluor 594-conjugated secondary Ab. The same slide was also treated with DAPI for the staining of nuclei. (B) The transfected HeLa cell with activated TICAM-1, whereas (C) shows a cell with inactive TICAM-1. (D) TICAM-1 RHIM mt was transfected into HeLa cells instead of TICAM-1 WT. (E) TICAM-1 N+TIR P434H was transfected into HeLa instead of TICAM-1 WT. The transfection and staining conditions were identical to those in (B). An enlarged scale of the area within the white square in the merged image in (B) and (D) is shown to the right of the image.

recruited BS69 (Fig. 2D), whereas TICAM-1 N+TIR P434H failed to recruit BS69 in the cytoplasm (Fig. 2E).

Translocation of BS69 in response to TICAM-1 signaling

To observe the nucleus-to-cytoplasm shuttling of BS69, HEK293T cells were transfected with the FLAG-BS69 and HA-TICAM-1 plasmids, and 24 h later the cells were solubilized to separate the nuclei and cytoplasm. Each fraction was further solubilized and immunoprecipitated with anti-FLAG and anti-HA Ab (Fig. 3A). The cytoplasmic fraction did not contain any detectable lamin A, suggesting that nuclear contamination in the cytoplasmic fraction was negligible (Fig. 3A center panel). TICAM-1 over-expression clearly allowed some BS69 to move to the cytoplasm (Fig. 3A). The dynamics of BS69 translocation in response to TICAM-1 stimulation was then examined using polyI:C as a TLR3/TICAM-1 stimulator [1]. Cytoplasmic BS69 was detected 3 h after

polyI:C stimulation in both HeLa (Fig. 3B) and HEK293T cells (Fig. 3C). Imaging analysis using the polyI:C-stimulated cells indicated that cytoplasmic speckle formation of BS69 and TICAM-1 also appeared 3 h after polyI:C stimulation (Fig. 3D). PolyI:C stimulation barely altered the BS69 mRNA levels (data not shown). Hence, BS69 moves from the nucleus to the cytoplasm in association with the activation and oligomerization of TICAM-1.

BS69 is a positive regulator of the TICAM-1 pathway

We next examined if the TICAM-1 signal was enhanced by transfected BS69. NF-κB activation was up-regulated by the over-expression of BS69 (Fig. 4A). PolyI:C-dependent induction of IFN-β luciferase was also enhanced by the transfection and expression of BS69 in HEK293T and HeLa cells (Fig. 4B and C). IFN-β mRNA levels

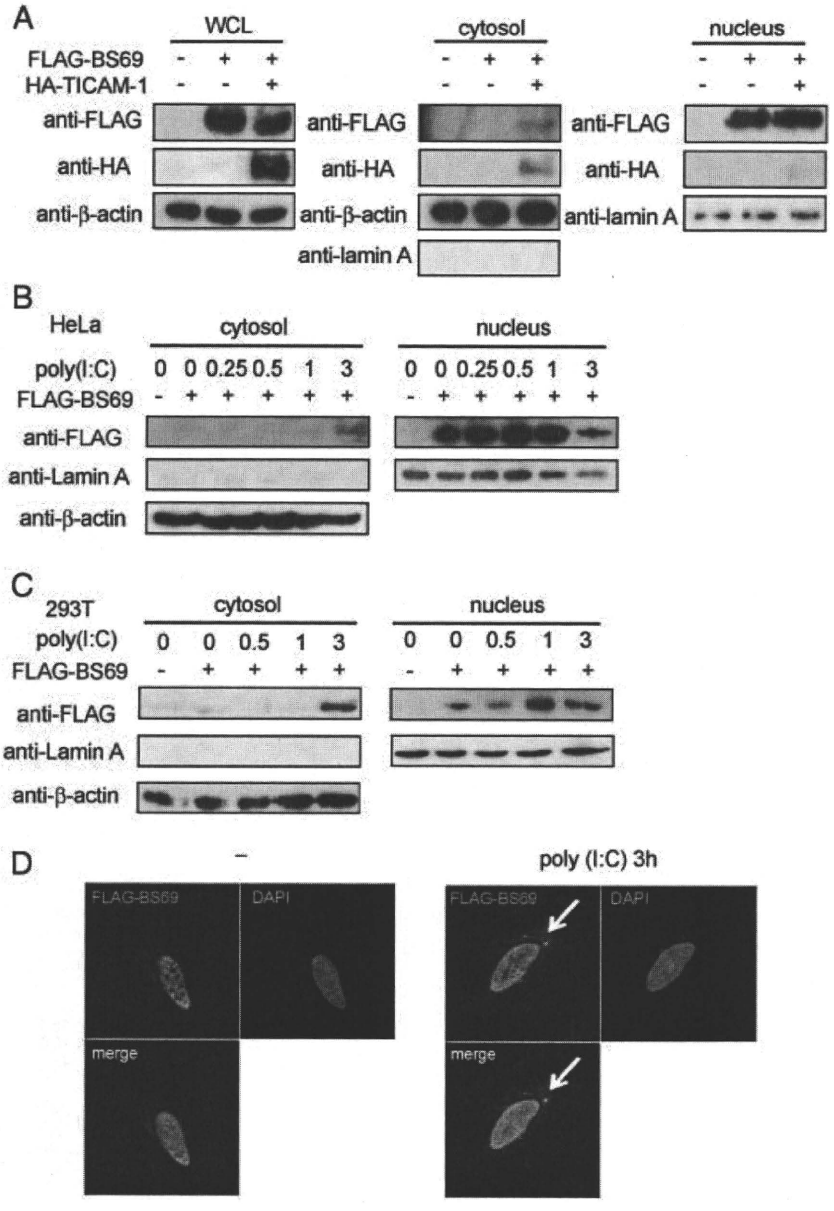

Figure 3. TICAM-1 over-expression induces cytoplasmic translocation of BS69. (A) HEK 293T cells were transfected with 1 ng of pEF-BOS HA-TICAM-1 WT and 100 ng of pEF-BOS FLAG BS69. After 24 h, the cells were lysed and cytoplasmic and nuclear extractions were prepared. Each extraction was resolved by SDS-PAGE and immunoblotted with either anti-HA, anti-FLAG anti-β-actin or anti-Lamin A (as a nuclear marker) Ab. (B) HeLa cells were transfected with 1 μg of pEF-BOS FLAG-BS69. After 24 h, the cells were stimulated with 10 μg/mL of polyI:C for either 0, 0.25, 0.5, 1 or 3 h. The cytoplasmic and nuclear extractions were then prepared, run on SDS-PAGE gels and immunoblotted with either anti-FLAG, anti-β-actin or anti-Lamin A (as a nuclear marker) Ab. (C) HEK293T cells were transfected with 100 ng of pEF-BOS FLAG-BS69 and 100 ng of pEF-BOS human TLR3. After 24 h, the cells were stimulated with 50 μg/mL of polyI:C for the indicated periods. The cytosolic and the nuclear extractions were analyzed as shown in (B). (D) HeLa cells were transfected with 400 ng of pEF-BOS FLAG-BS69. After 24 h, the cells were stimulated with 10 μg/mL of polyI:C for 3 h. Thereafter, the cells were fixed and stained with anti-FLAG Ab and visualized with Alexa Fluor 594-conjugated secondary Ab. The same slide was also treated with DAPI for the staining of nuclei. The white arrows indicate BS69 cytoplasmic speckles.

were quantitatively measured in cells expressing BS69 after polyI:C stimulation (Fig. 4D). The levels of mRNA significantly increased at 6 and 12 h after polyI:C stimulation in the BS69-transfected cells in comparison with cells containing the control vector. We next introduced an siRNA of BS69 into HeLa cells and examined polyI:C-mediated IFN-β induction. The IFN-β mRNA level induced by polyI:C dropped down by the presence of the siRNA (Supporting Information Fig. S1). The data suggest that BS69 acts as a positive regulator of the TICAM-1 pathway in both NF-κB activation and IFN-β induction through its trafficking from the nucleus to the cytoplasm.

Discussion

We demonstrated in this study that BS69 binds TICAM-1 and positively modulates the function of TICAM-1 in terms of NF-κB and IRF-3 activation. BS69 is essentially a nuclear protein that can be displaced from the nucleus to the cytoplasm to regulate TICAM-1 signaling. Either low doses of polyI:C stimulation or TICAM-1 expression induces BS69 translocation, whereas high TICAM-1 expression leads to the disappearance of the nuclear and cytosolic BS69, presumably due to apoptosis (data not shown). BS69 not only augments the TICAM-1 pathway *via* its binding to TCAM-1, but also participates in BS69 nucleus-to-cytoplasm displacement.

BS69 is a 74-kDa protein with three truncated isoforms that are formed through alternative splicing [5]. All four forms are unstable as they can be easily degraded by post-translational modification through the proteasome pathway [5]. Our preliminary data suggest that protein modification, particularly one other than ubiquitination, participates in the degradation of BS69 (data not shown). This is consistent with the finding that high doses of TICAM-1 induce the activation of TRAF E3 ligases [11] and protein modification [12], though the mechanisms have yet to be determined.

The previous reports have demonstrated that BS69 physically binds EBV-derived LMP1 and negatively regulates the canonical NF-κB activation by LMP1 [10, 13]. Although the regulatory mode of LMP1 is reciprocal to that of TICAM-1, the extranuclear displacement of BS69 commonly occurs in polyI:C- and LMP1-activating pathways. Thus, BS69 exerts a functional modulation of NF-κB in at least in two cytoplasmic pathways: positive regulation in the TICAM-1 pathway and negative regulation in the LMP1 pathway.

TICAM-1 recruits TRAF1, TRAF2 and TRAF6 to sites within its N-terminal region [11], and TRAF3 indirectly couples with the

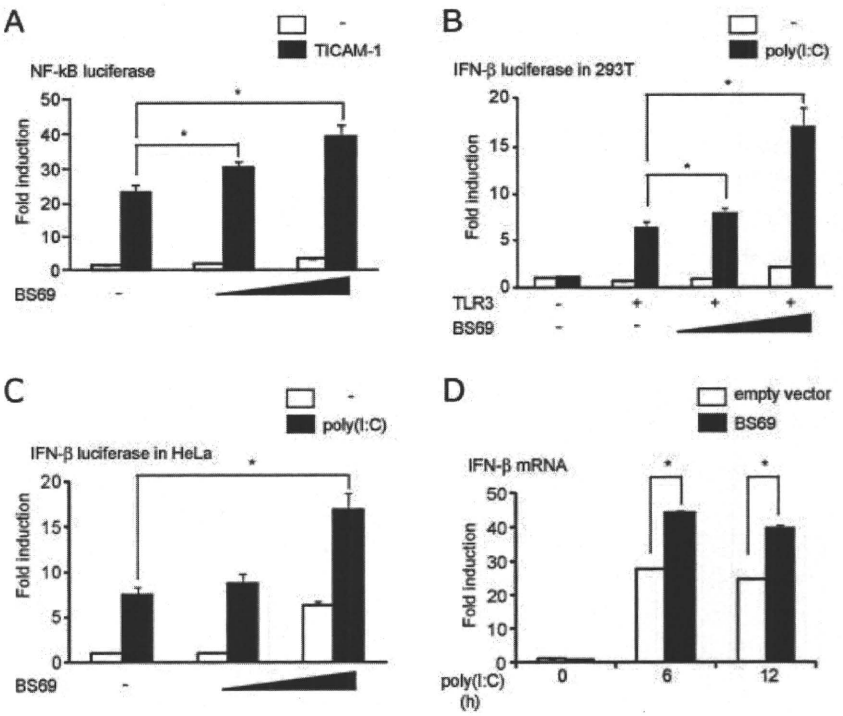

Figure 4. BS69 is a positive regulator of the TICAM-1 pathway. (A) HEK 293T cells in 24-well plates were transfected with pEF-BOS FLAG-BS69 (10, 100 ng) together with pEF-BOS HA-TICAM-1 WT (100 ng), the NF-κB reporter (100 ng) and phRL-TK (5 ng). Twenty-four hours after transfection, the luciferase reporter activity was measured. The average activities from three independent assays are shown as fold induction. (B) HEK 293T cells were transfected with pEF-BOS FLAG-BS69 (10, 100 ng) together with pEF-BOS TLR3 (10 ng), the IFN-β promoter reporter (100 ng) and phRL-TK (5 ng). After 24 h, the cells were stimulated with 10 μg/mL polyI:C for 6 h and the luciferase reporter activity was then measured. The average activities from three independent assays are shown as fold induction. (C) HeLa cells in 24-well plates were transfected with pEF-BOS FLAG-BS69 (10,100 ng) together with the IFN-β promoter reporter (100 ng) and phRL-TK (5 ng). Twenty-four hours after transfection, the cells were stimulated with 10 μg/mL polyI:C for 6 h, and then the luciferase reporter activity was measured. The average activities from three independent assays are shown as fold induction. (D) HeLa cells in 12-well plates were transfected with either pEF-BOS FLAG-BS69 (1 μg) or empty vector (1 μg). After 24 h, the cells were stimulated with 10 μg/mL polyI:C for the indicated time periods. The IFN-β mRNA levels were determined by real-time PCR. *$p<0.05$.

molecular complex of these proteins [14, 15]. NAP1 also bind indirectly to the N-terminus of TICAM-1 [3]. Thus, the visible TICAM-1 multimer observed by confocal analysis is likely a signal platform directing the activation of IRF-3-activating kinases and IκB degradation kinases [4]. From our data, we can infer that when an optimal stimulus, such as an RNA viral infection, is present in the target cells, two molecular events are independently triggered: BS69 translocation to the cytoplasm and TICAM-1 signalosome formation. These two events could be simultaneously reproduced in our system, resulting in the up-regulation of the TICAM-1 inflammatory pathway.

Upon infection of a cell by EBV, the EBV product LMP1 induces NF-κB and JNK activation. This LMP1-derived NF-κB activation is negatively regulated by BS69 [10] coping with internal TLR3 signaling. Radical activation of the TICAM-1 pathway, however, is not supported by BS69-mediated NF-κB up-regulation as BS69 is degraded *via* post-translational modification. This is in accordance with the fact that full length TICAM-1 occasionally induces apoptotic cell death, which reflects a natural feature of the antiviral response.

The previous studies have demonstrated that BS69 acts as a transcriptional repressor in association with a variety of transcription factors such as c-Myb, B-Myb, Ets2 and MGA [7, 16, 17]. BS69 has also been shown to repress transcription by recruiting N-CoR [6]. A recent study suggested that BS69 has another role in gene repression since it co-precipitates with a set of chromatin remodeling factors and interacts with the transcription factor ZHX1 [18]. Furthermore, BS69 has been shown to associate with mitotic chromosomes and to interact with Brg1 (the catalytic subunit of the mammalian SWI/SNF complex), indicating an additional role of BS69 in chromatin remodeling [19]. In either case, it is clear that BS69 functions in the nucleus. As a sensitive Ab against BS69 is not available, it is extremely difficult to detect endogenous BS69 protein in the cytoplasm. However, our studies, together with a report on BRAM1, a truncated form of BS69 which displaces TRADD from LMP1 to inhibit LMP1-mediated NF-κB activation [10], indicate that BS69 plays a role in the cytoplasm to modulate inflammation secondary to viral infection. In keeping with its NF-κB modulating function and chromatin-associated properties, BS69 is a bifunctional protein acting in the nucleus and cytoplasm to maintain the homeostasis of the cellular environment.

In mDC, TICAM-1 has a unique role in driving cellular immunity as $CD8^+$ T, $CD4^+$ Treg, Th1, Th17 and NK cells are all activated in response to TICAM-1-mediated mDC maturation [1, 20]. We found the TICAM-1 pathway in mDC is activated *via* endosomal TLR3 through the phagocytic uptake of viral-infected cell debris [21]. Our data suggest the possibility that BS69 is an agent used to regulate the induction of TICAM-1-mediated cellular immunity in addition to the NF-κB- and IFN-activating pathways. More detailed analysis of endogenous TLR-associated proteins and BS69/BRAM1, including *in vivo* functional analysis, will be needed in order to highlight the precise cytoplasmic function(s) of BS69.

Materials and methods

Cell culture and reagents

HEK293 T cells were maintained in DMEM supplemented with 10% heat-inactivated FBS and antibiotics. HeLa cells were cultured in Eagle's MEM with 10% heat-inactivated FBS and L-glutamine. The following Ab were obtained commercially: anti-FLAG, anti-HA and anti-β-actin (Sigma-Aldrich); anti-Myc (Santa Cruz); anti-Lamin A (Cell Signaling Technology). Alexa Fluor 488- and Alexa Fluor 568-conjugtaed secondary Ab were from Invitorgen Life Technologies. polyI:C was from Amersham Biosciences.

Plasmids

Complementary DNA from human TLR3, TICAM-1WT, TICAM-1 N+TIR P434H and RHIM mt were cloned in our laboratory by RT-PCR and ligated into the cloning site of the expression vector, pEF-BOS and pcDNA4 Myc-HisA [4]. BS69 cDNA was cloned as described previously [11]. Mutations were introduced by site-directed mutagenesis using PCR. [3]. All constructs were confirmed by sequencing.

Confocal microscopy

HeLa cells (2.5×10^4 cells/well) were plated on a micro cover glass (Matsunami Glass) in 12-well plate. The following day, cells were transfected with the indicated plasmids using FuGENE HD (Roche). The total amounts of DNA were kept constant by adding empty vector. After 24 h, cells were fixed in acetone and blocked in PBS containing 1% BSA and then labeled with the indicated primary Ab for 1 h at room temperature. Alexa Fluor 488- or Alexa Fluor 594-conjugtaed secondary Ab were used for the visualizing proteins detected by the primary Ab. For nucleus staining, cells were treated with DAPI in PBS. After all staining procedures were finished, micro cover glasses were mounted onto a slide glass using PBS containing 2.3% DABCO and 50% glycerol. Cells were visualized at × 63 magnification under an LSM510 META microscope (Zeiss).

Reporter gene assay

Cells were seeded onto 24-well plates and transfected with various amounts of expression vectors, the reporter gene and the phRL-TK control plasmid using FuGene HD (Roche) according to the manufacturer's instructions. After 24 h, the cells were harvested in 50 μL lysis buffer. The luciferase activity was measured using Dual-Luciferase Reporter assay systems (Promega) and was shown as the means ± SD of three experiments.

Western blotting and immunoprecipitation assay

For whole cell lysis, cells were solubilized in the SDS sampling buffer (50 mM Tris-HCl, pH 6.8, 2% SDS, and 10% glycerol, 32% Urea) and then sonicated for 5 min. For cytosol extraction, cells were solubilized in the lysis buffer A (10 mM HEPES-KOH, pH 7.9, 150 mM NaCl, 15 mM $MgCl_2$, 10 mM KCl, 40 mg/mL digitonin, protease inhibitor cocktail, 0.1 mM PMSF, 50 mM NaF and 1 mM Na_3VO_4) on ice for 30 min and then centrifuged at 10 000 × *g* for 1 min at 4°C. The supernatant was collected as a cytosol extraction. After centrifugation, the nuclei-containing pellet was resuspended in the buffer C (50 mM HEPES-KOH (pH 7.9), 420 mM KCl, 1.5 mM $MgCl_2$, 1 mM EDTA, 2% glycerol, protease inhibitor cocktail, 0.1 mM PMSF, 50 mM NaF and 1 mM Na_3VO_4) at 4°C for 30 min. The suspension was pelleted by centrifugation and the supernatants were collected as a nuclear extraction. The supernatants were separated by SDS-PAGE, and the gel was transferred onto polyvinylidene difluoride membranes. The membranes were then blocked with TBS, pH 8.0, containing 5% skim milk, immunoblotted with specific Ab and visualized with the appropriate horseradish peroxidase-conjugated secondary Ab using the ELC plus Western Blotting Detection System (Amersham Pharmaica). For immunoprecipitation, cells were lysed in the TritonX-100 lysis buffer (50 mM Tris-HCl, pH 7.4, 150 mM NaCl, 1.5 mM $MgCl_2$, 1% TritonX-100, 10% glycerol, protease inhibitor cocktail, 0.1 mM PMSF, 50 mM NaF and 1 mM Na_3VO_4) and then centrifuged at 12 000 × *g* for 10 min at 4°C. The supernatants were incubated with anti-FLAG or anti-Myc Ab and protein G-Sepharose (Amersham Pharmacia) for overnight at 4°C. The immunoprecipitates were collected by centrifugation, washed four times in the lysis buffer and then analyzed by SDS-PAGE.

RNA purification and real-time PCR

Total RNA was prepared using TRIzol Reagent (Invitrogen) following the manufacturer's instructions. RT-PCR was carried out using the High Capacity cDNA Reverse Transcripition kit (Applied Biosystems) according to the manufacturer's instructions. The following oligonucleotides were used for human β-actin: 5′-CCT GGC ACC CAG CAC AAT-3′ and 5′-GCC GAT CCA CAC ACG GAG TAC T-3′; and for human IFN-β: 5′-TGG GAG GAT TCT GCA TTA CC-3′ and 5′-CAG CAT CTG CTG GTT GAA GA-3′; and for human BS69: 5′-GTC CAC GGT ATG CAC CCT AAA GAG and 5′-AAC ACC TCT CCA GGC AAA TGG. IFN-β mRNA were normalized to β-actin and fold inductions of transcripts were calculated using the δδCT method relative to unstimulated HeLa cells.

Yeast two-hybrid screening

The yeast two-hybrid assay was performed as described previously [12]. The yeast AH109 strain (Clontech, Palo Alto, CA, USA) was transformed using bait (pGBKT7) and prey (pGADT7) plasmids. The transformants were streaked onto plates and incubated for 3–5 days. and in the figures represent the bait and prey plasmid, respectively. The various BD-TICAM-1 and AD-BS69 were constructed by inserting each cDNA fragment into the pGBKT7 (bait) or pGADT7 (prey) plasmids (Clontech). SD-WLH is a yeast synthetic dextrose medium that lacks Trp, Leu and His aa. SD-WLHA lacks adenine in addition to Trp, Leu and His.

Gene silencing

Knockdown of BS69 was carried out using siRNA, BS69 siRNA-1: 5′-GGA UAU UGG CCA GGA GTT-3′, BS69 siRNA-2: 5′-CGG UAU GCA CCC UAA AGA GTT-3′ and control siRNA: 5′-GGG AAG AUC GGG UUA GAC UUC-3′. In total, 20 pmol of each siRNA was transfected into HeLa cells in 24-well plate with Lipofectamin 2000 according to the manufacture's protocol. Knockdown of BS69 was confirmed 48 h after siRNA transfection. Experiments were repeated twice for confirmation of the results. One of the two siRNA, BS69 siRNA-1 was effective in BS69 gene silencing. Typically, 6 h after polyI:C (10 μg/mL) stimulation, the level of the BS69 mRNA was determined by real-time PCR as described in RNA purification and real-time PCR section.

Acknowledgements: The authors thank the members of our laboratory for invaluable discussions. This work was supported in part by the Program of Founding Research Centers for Emerging and Reemerging Infectious Diseases, MEXT, Sapporo Biocluster "Bio-S", the Knowledge Cluster Initiative of the MEXT, Grants-in-Aid from the Ministry of Education, Science, and Culture (Specified Project for Advanced Research) and the Ministry of Health, Labor, and Welfare of Japan, Mitsubishi Foundation, Mochida Foundation, NorthTec Foundation and Yakult Foundation. M. S. was supported by Reseach Fellow of the Japan Sciety for the Promotion of Science. Dr. Greg Newton (NEWTONediting) reviewed the manuscript.

Conflict of interest: The authors declare no financial or commercial conflict of interest.

References

1 **Matsumoto, M. and Seya, T.,** TLR3: interferon induction by double-stranded RNA including poly(I:C). *Adv. Drug Deliv. Rev.* 2008. **60**: 805–812.

2 **Matsumoto, M., Funami, K., Tanabe, M., Oshiumi, H., Shingai, M., Seto, Y., Yamamoto, A. and Seya, T.,** Subcellular localization of Toll-like receptor 3 in human dendritic cells. *J. Immunol.* 2003. **171**: 3154–3162.

3 **Funami, K., Sasai, M., Ohba, Y., Oshiumi, H., Seya, T. and Matsumoto, M.,** Spatiotemporal mobilization of Toll/1L-1 receptor domain-containing

adaptor molecule-1 in response to dsRNA. *J. Immunol.* 2007. **179**: 6867–6872.

4 **Funami, K., Sasai, M., Oshiumi, H., Seya, T. and Matsumoto, M.,** Homo-oligomerization is essential for Toll/IL-1 receptor domain containing adaptor molecule-1-mediated NF-kappaB and interferon regulatory factor-3 activation. *J. Biol. Chem.* 2008. **283**: 18283–18291.

5 **Velasco, G., Grkovic, S. and Ansieau, S.,** New insights into BS69 functions. *J. Biol. Chem.* 2006. **281**: 16546–16550.

6 **Masselink, H. and Bernards, R.,** The adenovirus E1A binding protein BS69 is a corepressor of transcription through recruitment of N-CoR. *Oncogene* 2000. **19**: 1538–1546.

7 **Ladendorff, N. E., Wu, S. and Lipsick, J. S.,** BS69, an adenovirus E1A-associated protein, inhibits the transcriptional activity of c-Myb. *Oncogene* 2001. **20**: 125–132.

8 **Ansieau, S. and Leutz, A.,** The conserved Mynd domain of BS69 binds cellular and oncoviral proteins through a common PXLXP motif. *J. Biol. Chem.* 2002. **277**: 4906–4910.

9 **Izumi, K. M., Cahir McFarland, E. D., Ting, A. T., Riley, E. A., Seed, B. and Kieff, E. D.,** The Epstein-Barr virus oncoprotein latent membrane protein 1 engages the tumor necrosis factor receptor-associated proteins TRADD and receptor-interacting protein (RIP) but does not induce apoptosis or require RIP for NF-κB activation. *Mol. Cell. Biol.* 1999. **19**: 5759–5767.

10 **Ikeda, O., Sekine, Y., Mizushima, A., Oritani, K., Yasui, T., Fujimuro, M., Muromoto, R. *et al.*,** BS69 negatively regulates the canonical NF-kappaB activation induced by Epstein-Barr virus-derived LMP1. *FEBS Lett.* 2009. **583**: 1567–1574.

11 **Sasai, M., Oshiumi, H., Funami, K., Matsumoto, M. and Seya, T.,** Direct binding of TRAF2 and TRAF6 to TICAM-1/TRIF adaptor of the Toll-like receptor 3/4 pathway. *Mol. Immunol.* 2009, in press.

12 **Oshiumi, H., Matsumoto, M., Funami, K., Akazawa, T. and Seya, T.,** TICAM-1, an adapter molecule that participates in Toll-like receptor 3-mediated interferon-beta induction. *Nat. Immunol.* 2003. **4**: 161–167.

13 **Wan, J., Zhang, W., Wu, L., Bai, T., Zhang, M., Lo, K. W., Chui, Y. L. *et al.*,** BS69, a specific adaptor in the latent membrane protein1-mediated c-Jun N-terminal kinase pathway. *Mol. Cell. Biol.* 2006. **26**: 448–456.

14 **Häcker, H., Redecke, V., Blagoev, B., Kratchmarova, I., Hsu, L. C., Wang, G. G., Kamps, M. P. *et al.*,** Specificity in Toll-like receptor signalling through distinct effector functions of TRAF3 and TRAF6. *Nature* 2006. **439**: 204–207.

15 **Oganesyan, G., Saha, S. K., Guo, B., He, J. Q., Shahangian, A., Zarnegar, B., Perry, A. and Cheng, G.,** Critical role of TRAF3 in the Toll-like receptor-dependent and -independent antiviral response. *Nature* 2006. **439**: 208–211.

16 **Wei, G., Schaffner, A. E., Baker, K. M., Mansky, K. C. and Ostrowski, M. C.,** Ets-2 interacts with co-repressor BS69 to repress target gene expression. *Anticancer Res.* 2003. **23**: 2173–2178.

17 **Masselink, H., Vastenhouw, N. and Bernards, R.,** B-myb rescues ras-induced premature senescence, which requires its transactivation domain. *Cancer Lett.* 2001. **171**: 87–101.

18 **Ogata-Kawata, H., Yamada, K., Uesaka-Yoshino, M., Kagawa, N. and Miyamoto, K.,** BS69, a corepressor interacting with ZHX1, is a bifunctional transcription factor. *Front. Biosci.* 2007. **12**: 1911–1926.

19 **Ekblad, C. M., Chavali, G. B., Basu, B. P., Freund, S. M., Veprintsev, D., Hughes-Davies, L., Kouzarides, T. *et al.*,** Binding of EMSY to HP1beta: implications for recruitment of HP1beta and BS69. *EMBO Rep.* 2005. **6**: 675–680.

20 **Seya, T. and Matsumoto, M.,** The extrinsic RNA-sensing pathway for adjuvant immunotherapy for cancer. *Cancer Immunol. Immunother.* 2009. **58**: 1175–1184.

21 **Ebihara, T., Shingai, M., Matsumoto, M., Wakita, T. and Seya, T.,** Hepatitis C virus (HCV)-infected hepatocytes extrinsically modulate dendritic cell maturation to activate T cells and NK cells. *Hepatology* 2008. **48**: 48–58.

Abbreviations: **BS69:** adenovirus 5 E1A-binding protein · **IRF:** IFN-regulatory factor · **LMP1:** latent membrane protein 1 · **mDC:** myeloid dendritic cells · **mt:** mutant · **TICAM-1:** Toll-interleukin 1 receptor domain (TIR)-containing adaptor molecule-1

Full correspondence: Dr. Tsukasa Seya, Department of Microbiology and Immunology, Hokkaido University Graduate School of Medicine, Kita 15, Nishi 7, Kita-ku Sapporo 060-8638, Japan
Fax: +81-11-706-7866
e-mail: seya-tu@pop.med.hokudai.ac.jp

Current address: Miwa Sasai, Department of Immunobiology, Yale University School of Medicine, New Haven, CT 06510, USA

Supporting Information for this article is available at www.wiley-vch.de/contents/jc_2040/2009/39878_s.pdf

Received: 6/8/2009
Revised: 3/9/2009
Accepted: 3/9/2009

ISOLATION AND CHARACTERIZATION OF RNA APTAMERS SPECIFIC FOR THE HUMAN TOLL-LIKE RECEPTOR 3 ECTODOMAIN

Tomoya Watanabe[1], Kiyoharu Ito[2], Misako Matsumoto[2], Tsukasa Seya[2], Kotomi Hatakeyama[1], Satoshi Nishikawa[3], Tsunemi Hasegawa[1], and Kotaro Fukuda[1*]

[1]Department of Material and Biological Chemistry, Faculty of Science, Yamagata University, Yamagata 990-8560, Japan.

[*]Corresponding author: Kotaro Fukuda

FAX: 023-628-4604; E-mail: kotaro.f@sci.kj.yamagata-u.ac.jp

[2]Department of Microbiology and Immunology, Graduate School of Medicine, Hokkaido University, Sapporo 060-8638, Japan.

[3]Age Dimension Research Center, National Institute of Advanced Industrial Science and Technology (AIST), Tsukuba 305-8566, Japan.

(Received March 10, 2009; Accepted June 1, 2009)

(Abstract)

Toll-like receptor 3 (TLR3) detects double-stranded RNA (dsRNA), known to be a universal viral molecular pattern, and activates the antiviral immune response. While TLR3 preferentially recognizes polyinosinic-polycytidylic acid (poly(I:C)), no sequence-specific dsRNA has been shown to activate TLR3. To determine whether TLR3 preferentially recognizes a specific RNA sequence or structure that acts upon the TLR3 signaling pathway, *in vitro* selection against the human TLR3 ectodomain (TLR3 ECD) was performed. After the seventh selection cycle, two major classes, Family-I and Family-II, emerged from 64 clones with binding constants of about 3 nM. To examine the structure–function relationship of Family-I and -II aptamers, mutational analyses and RNase mapping were carried out. Furthermore, to elucidate the effect of selected aptamers on TLR3 signaling *in vivo*, a reporter gene assay was conducted in cells. These aptamers did not have any agonistic or antagonistic effects on TLR3 signaling in TLR3-transfected HEK293 cells, although they bound to TLR3 ECD with high affinity *in vitro*. These results suggest that selection of RNA aptamers for TLR3 ECD should be performed under physiological conditions, since TLR3 ECD localizes in acidic compartments such as endosomes.

(Keywords)

Toll-like receptor 3, TLR3 ectodomain, RNA aptamer, *in vitro* selection, SELEX

1. Introduction

Toll-like receptors (TLRs) play central roles in the innate immune response by recognizing conserved structural patterns in diverse microbial molecules [1]. All TLRs are type I integral membrane glycoproteins composed of an ectodomain (ECD) linked by a transmembrane domain to a cytoplasmic signaling Toll/IL-1 receptor (TIR) domain [2]. Ligand recognition by TLRs is mediated through their N-terminal ECD, which contains varying numbers of leucine-rich repeats (LRRs) [3]. More than 10 TLRs have been identified in human and mouse [4]. TLR1, TLR2, TLR4, TLR5, and TLR6 recognize bacterial cell wall and cell surface components, such as lipoproteins, lipopolysaccharide, and flagellin. In contrast, TLR3, TLR7, TLR8, and TLR9 recognize pathogen nucleic acids, such as viral RNAs and bacterial DNA [4,5]. TLR3 recognizes double-stranded RNA (dsRNA) derived from viral genomes and replication intermediates and recruits TIR-containing adaptor molecule (TICAM)-I (also called TIR-containing adaptor inducing interferon (IFN)-β, TRIF), leading to the production of IFN-β and inflammatory cytokines [6,7]. As these immune responses are essential for combating viral invasions, TLR3 plays a key role in antiviral immunity. On the other hand, it is known that West Nile virus infection leads to a TLR3-dependent inflammatory response, which is involved in brain penetration of the virus and neuronal injury [8]. The three-dimensional structure of the human TLR3 ECD, which contains the dsRNA-binding region, has been reported by two groups [9,10]. TLR3 ECD resembles a horseshoe-shaped solenoid of 23 LRRs, with each LRR forming one turn of the solenoid. Furthermore, a recent report revealed the crystal structure of TLR3 ECD bound to a dsRNA ligand [11]. Each TLR3 ECD binds to a dsRNA at two sites located at opposite ends of the TLR3 horseshoe, and an intermolecular interaction between the two TLR3 ECD C-terminal domains coordinates and stabilizes the dimer formation.

Nucleic acid-sensing TLRs, TLR3, TLR7, TLR8, and TLR9, are localized in the endosome [12,13]. It has been reported that TLR7 and TLR8 (receptors for single-stranded RNA), as well as TLR9 (a receptor for CpG oligodeoxyribonucleotide), respond to their ligands in a sequence-dependent manner [14]. Although polyinosinic-polycytidylic acid (poly(I:C)), a synthetic dsRNA analogue, is a potent inducer of TLR3 signaling, no sequence-specific inducer or inhibitor for TLR3 is known. Anti-inflammatory drugs (TLR3 antagonists) and adjuvants for vaccines (TLR3 agonists) that regulate TLR3 signal transduction could be important for the development of future therapeutic treatments. Therefore, to investigate whether TLR3 recognizes and responds to specific dsRNA, *in vitro* selection against TLR3 ECD was carried out. *In vitro* selection (SELEX) is a powerful tool for obtaining RNA ligands that bind to a target molecule with high affinity and specificity [15,16]. So far, high-affinity DNA or RNA ligands for target molecules including proteins, organic dyes, and amino acids have been isolated by *in vitro* selection [17]. Because binding of

an aptamer to its target is a highly specific interaction that involves discrimination between related proteins that share common sets of structural domains, aptamers represent a potentially attractive class of molecules for therapeutic compounds. Furthermore, RNA aptamers against RNA-binding proteins (RBPs) are useful for dissecting the interactions between RNA and protein, and such aptamers could potentially modulate the function of target RBPs.

This report describes the isolation and characterization of RNA aptamers that bind with high specificity to human TLR3 ECD. Application of TLR3 ECD aptamers *in vivo* is also described to estimate their agonistic and antagonistic effects on TLR3 signaling.

2. Materials and Methods

2.1. Protein and nucleic acids

TLR3 ECD with an N-terminal FLAG tag and C-terminal His tag (TLR3-ECD) was expressed using a baculovirus system and purified as described previously [18]. The starting RNA pool of N40H for *in vitro* selection has the sequence 5'-GGUAGAUACGAUGGA–(N40)–CAUGACGCG CAGCCA-3'. The antisense DNA template, 5'-TGGCTGCGCGTCATG–(N40)–TCCATCGTATC TACC-3' (10 pmol), was converted to dsDNA by PCR with a 5'-end primer, 5'-TGTAATACGACTCACTATAGGTAGATACGAT GGA-3' (40 pmol). Underlined letters in the 5'-end primer indicate the T7 RNA promoter sequence. PCR was carried out for six cycles, and dsDNA was recovered by ethanol precipitation. The dsDNA (50 pmol) was reamplified by PCR with the 5'-end primer and a 3'-end primer, 5'-TGGCTGCGCGTCATG -3' (100 pmol each). After 20 cycles of PCR, the amplified DNA pool was recovered by ethanol precipitation. T7 RNA transcription was performed with at least 100 pmol of the DNA pool using the T7 AmpliScribe Kit (Epicentre Technologies). The transcribed RNA was then purified on 8% denaturing PAGE. The final yield of the random RNA pool N40H was approximately 70 μg.

Family-I and -II aptamer mutants were constructed by PCR mutagenesis using mutagenic primers and template DNA. The DNA sequences of these mutants were confirmed by an Applied Biosystems model 3100 automatic sequencer (Applied Biosystems).

2.2. *In vitro* selection of RNA aptamers for TLR3-ECD

In vitro selection was carried out essentially as reported previously [19]. For the first cycle of selection, the N40H RNA pool (500 pmol) was incubated with 62.5 pmol of TLR-ECD in 50 μl of binding buffer [2 mM HEPES-NaOH (pH 7.6), 3 mM $MgCl_2$, and 100 mM NaCl] at room temperature for 1 h. The binding reaction was separated by filtration through a nitrocellulose filter (HAWP filter, 0.45 μm) fitted in a pop-top filter holder (Nucleopore) and washed with 1 mL of binding buffer. The filter was eluted with 200 μl of elution buffer [0.4 M sodium acetate (pH 5.5), 5 mM EDTA (pH 8.0), and 7 M urea] at 90°C for 5 min. The eluted RNA was recovered by ethanol precipitation and reverse-transcribed using RevertAid™ M-MuLV Reverse Transcriptase (Fermentas) at 42°C for 1 h. The cDNA product was amplified by PCR and transcribed *in vitro* using the T7 AmpliScribe Kit (Epicentre Technologies). The product of this reaction was subjected to another cycle of selection for a total of 10 cycles. To specifically enrich the RNA pool for high-affinity ligands for TLR-ECD, the concentration of TLR-ECD and the RNA ligand were manipulated for each selection cycle (Table 1). Yeast tRNA (Boehringer Mannheim) was used as a non-specific competitor during the selection process.

The PCR product of the seventh selection cycle was introduced into the TA cloning vector (Invitrogen). After subcloning and transformation into *E. coli*, plasmid DNA was isolated from

Table 1. TLR3-ECD aptamer selection and binding analysis. TLR3-ECD, RNA pool, and competitor tRNA concentrations used during the selection step (total volume, 50 μL) of each generation are shown. The binding activity of the RNA pool at each cycle was analyzed by a filter binding assay with competitor tRNA (TLR3-ECD : RNA pool: tRNA = 0.05 : 0.05 : 2.5 μM) as described in the Materials and Methods. Binding activities were calculated as the percent of input RNA.

Generation No.	Concentration (μM)			Binding (%)
	TLR3-ECD protein	RNA pool	Competitor tRNA	
1	1.25	10.0	0.0	0
2	0.625	5.0	2.5	0.1
3	0.3	2.4	4.8	0
4	0.3	2.4	12.0	0.9
5	0.15	1.5	12.0	8.9
6	0.075	0.75	12.0	13.1
7	0.05	0.5	10.0	17
8	0.025	0.25	6.25	16
9	0.025	0.25	7.5	15
10	0.012	0.12	4.2	14

individual clones and the DNA sequences of 64 clones were analyzed with an Applied Biosystems model 3100 automatic sequencer (Applied Biosystems). The secondary structure models of selected aptamers, Family-I and -II, were drawn by the Mulfold program based on the Zuker algorithm [20].

2.3. Filter binding assay

The binding activity of the RNA pool was analyzed after each selection cycle. PCR products were internally transcribed *in vitro* with [α-^{32}P]CTP (Amersham), and the transcription product was tested by a filter binding assay using equimolar TLR-ECD and RNA and a 50-fold molar excess of non-specific competitor tRNA (TLR-ECD and RNA pool, 50 nM; tRNA, 2.5 μM) in binding buffer [2 mM HEPES-NaOH (pH 7.6), 3 mM $MgCl_2$, and 100 mM NaCl]. Radioactivity retained on the filter was counted with a BAS2000 image analyzer (Fuji Film). The binding activity was evaluated by calculating the percent of the input RNA retained on the filter in complexes with TLR-ECD (Table 1).

The equilibrium dissociation constants (K_D) for the selected aptamers, Family-I and -II, were determined by using a constant amount of internally labeled RNA aptamer (1 nM) in binding reactions with increasing concentrations of TLR-ECD (0.25–64 nM). Mixtures containing RNA and TLR-ECD were passed through a nitrocellulose filter and the filter was washed with 1 mL of binding buffer. The data points were fitted to a Scatchard plot to determine the equilibrium dissociation constant by Prism 4 ver 4.0b (GraphPad Software Inc.).

To analyze the binding ability of Family-I and -II mutants to TLR3-ECD, each ^{32}P-labeled mutant RNA (50 nM) was incubated with TLR3-ECD (50 nM) in 50 μl of binding buffer at 37°C for 1 h. The protein/RNA complex was separated by filtration on a nitrocellulose filter as described above. Radioactivity remaining on the filter was measured using a BAS2000 image analyzer (FujiFilm), and the amount of Family-I and -II mutants bound to TLR3-ECD was calculated as a percentage of the RNA input prior to filtration.

2.4. Structural analysis of RNA aptamers

For enzymatic probing, 5'-end-labeled Family-I and -II were partially digested with RNases T1 or A as previously reported with slight modifications [19], and the cleaved products were analyzed by 12% PAGE (7 M urea) with alkaline ladder of Family-I and -II.

2.5. Cell culture

For the expression of plasmids encoding human TLR3, HEK293 (human embryonic kidney) cells were used and cultured in DMEM cell culture medium (GIBCO) supplemented with 10% heat-inactivated fetal bovine serum (BIOSOURCE) and antibiotics (penicillin/streptomycin).

2.6. Reporter gene assay

HEK293 cells were seeded in 24-well plates (5 x 10^5 cells/well). Twenty-four hours later, the cells were transiently transfected with pEFBOS/TLR3 (0.1 μg) together with a p125-luc reporter (0.1 μg) and Renilla luciferase reporter (2.5 ng) in the presence of Lipofectamine 2000 (Invitrogen). The total amount of transfected plasmid (0.8 μg) was kept constant by adding empty vector. Twenty-four hours after transfection, the medium was replaced by fresh medium. RNA aptamer, poly(I:C) or both, was mixed with DOTAP Liposomal Transfection Reagent (3 μg/well; Roche) in OPTI-MEM (7 μl/well; Invitrogen) and pre-incubated for 15 min at R.T. The DOTAP/RNA complex was then transfected into cells and incubated. Cells were collected and washed twice with 1 ml of PBS buffer. The collected cells were then lysed using Passive Lysis Buffer (Promega), and the cell lysates were assayed for the dual luciferase activities (Promega). Data are expressed as mean relative stimulation SD for a representative experiment from independent experiments, performed in duplicate.

3. Results

3.1. Sequence and secondary structure of RNA aptamers specific for TLR3 ECD

To isolate high-affinity RNA ligands for TLR3 ECD, *in vitro* selection was carried out using an RNA library containing N40 random core sequences and recombinant TLR3-ECD protein. Initially, the randomized RNA pool (N40H), which consists of approximately 3 x 10^{14} molecules (500 pmol), was incubated with TLR3-ECD (62.5 pmol), and the RNA/TLR3-ECD complexes were separated from the unbound RNA molecules by passage through a nitrocellulose filter. The RNA retained on the filter was recovered, subjected to RT-PCR, transcribed by T7 RNA polymerase, and used for the next selection cycle. To specifically enrich the RNA pool for high-affinity ligands specific for TLR3-ECD, the concentrations of TLR3-ECD, RNA ligand, and competitor tRNA were manipulated for each selection cycle (Table 1). To confirm whether the selected RNA pools bind to TLR3-ECD, the binding activity of the RNA pools was evaluated by a filter binding assay after each selection cycle. The RNA pool from the seventh selection cycle (G7) had the highest affinity; about 17% of the total RNA pool bound to TLR3-ECD (Table 1).

To analyze the sequence and structural motifs in the G7 pool, we cloned the seventh-cycle PCR product into the TA vector and sequenced 64 clones. Although there were no conserved sequences among any of the clones, we were able to categorize them into 11 classes, from Family-I to -XI as shown in Table 2. Of these, two major classes emerged with entirely identical sequences: Family-I with 12 clones, followed by Family-II with 11 clones. We therefore focused on these Family-I and -II aptamers and proceeded to characterize them. When the secondary structures of the two aptamer classes were analyzed by the Mulfold program [20], we found that both

Table 2. Nucleotides sequences of RNA aptamers categorized into Family-I – Family-XI. Selected sequences from the G7 RNA pool are shown in uppercase. The fixed sequences for PCR primers are indicated in lowercase. Numbers in parentheses indicate the number of identical clones.

Family-I (12)	
gguagauacgaugga	UCAGGGUACCCCCUGUGGCCCGUCAACACAGGGGAAGUGG caugacgcgcagcca
Family-II (11)	
gguagauacgaugga	CUACCGCCACCCCGGGUCCGGGUGACGUUAAUUGAGGGCC caugacgcgcagcca
Family-III (4)	
gguagauacgaugga	ACAUGCCGGCAGGUGAGGCUGCACCUGUCUUUAAGGCGU caugacgcgcagcca
Family-IV (4)	
gguagauacgaugga	CCGGUCCCAGCGUUCAAGAGACCGGGGGCAGCAAGCAGU caugacgcgcagcca
Family-V (3)	
gguagauacgaugga	GGCAGCGAGGUGAAGCUGTAGUUAAGAAGACACCAACAGG caugacgcgcagcca
Family-VI (3)	
gguagauacgaugga	ACAAGAAUGGGCCCCGAGGUUCGUCAGCUGGGGGCAAGGG caugacgcgcagcca
Family-VII (3)	
gguagauacgaugga	CGGACGACCAUUGUCGAAGUAACCGUCGUCCGAAGCUGGC caugacgcgcagcca
Family-VIII (2)	
gguagauacgaugga	CGGAUCGUUCGCUCCCAGAAAGCGCGACUCUGAGGUUAAG caugacgcgcagcca
Family-IX (2)	
gguagauacgaugga	UACACAGCCGGCAGACGCGCUGUCGUUAACGCAGGCGAAA caugacgcgcagcca
Family-X (2)	
gguagauacgaugga	CCACAAAACCCGGCAGUCGGUGAGCAGGCCCACGAUCGGC caugacgcgcagcca
Family-XI (2)	
gguagauacgaugga	UCAACAAACAACAAAUACAAAGGCCCGUGCTACCGCGAAG caugacgcgcagcca
Others (16)	Orphan sequence

Family-I and -II aptamers were composed of three stem-loop (SL) structures, but we did not observe any sequence conservation or structural similarity between the two Families (Fig. 1).

3.2. Binding activity of Family-I and -II aptamers to TLR3 ECD

The equilibrium dissociation constant (K_D) of Family-I and -II aptamers was determined by a filter binding assay. Each aptamer (1 nM) was internally labeled and incubated with increasing concentrations of TLR3-ECD (0.25–64 nM) in the binding buffer. When the molar ratio of the RNA aptamers and TLR3-ECD was 1:64 (1 nM : 64 nM), approximately 27% maximal binding activity was observed (Fig. 2). The data points were fitted to a Scatchard plot to determine the equilibrium dissociation constant using Prism 4 ver 4.0b (GraphPad Software Inc.). The apparent K_D values for the aptamers were approximately 3 nM (Family-I, 2.1 nM; Family-II, 3.6 nM). Based on the K_D values for TLR3-ECD, selected Family-I and -II aptamers harbor high affinity for TLR3-ECD.

3.3. Enzymatic probing of Family-I and -II aptamers

The secondary structure models for Family-I and -II aptamers shown in Fig. 1 are based on Mulfold analysis of the RNA sequences. To confirm whether the solution structures of the two aptamer groups are consistent with the proposed secondary structure models, Family-I and -II aptamers were subjected to enzymatic probing using RNases T1 and A, which cleave adjacent to the 3'-phosphate of G

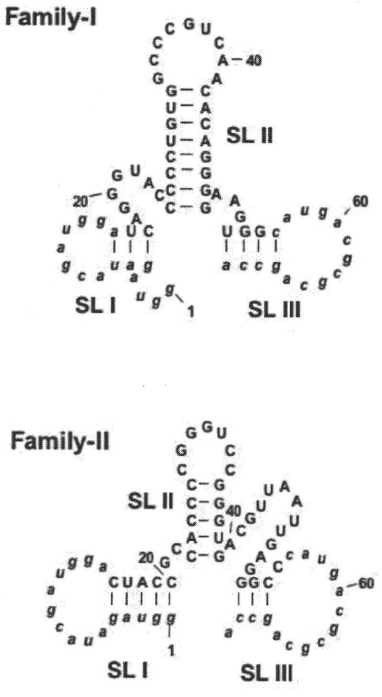

Figure 1. The secondary structure models of Family-I and -II aptamers against TLR3-ECD predicted by the Mulfold program [20]. Selected sequences are shown in normal letters. Lowercase letters indicate the constant sequence regions flanking the randomized N40 core. SL, stem–loop structure.